CHARACTERIZATION OF POLYURETHANE AT MULTIPLE SCALES FOR EROSION MECHANISMS UNDER SAND PARTICLE IMPACT

A Thesis

by

NIRMAL SHANKAR SIGAMANI

Submitted to the Office of Graduate Studies of
Texas A&M University
in partial fulfillment of the requirements for the degree of

MASTER OF SCIENCE

May 2010

Major Subject: Aerospace Engineering

CHARACTERIZATION OF POLYURETHANE AT MULTIPLE SCALES FOR EROSION MECHANISMS UNDER SAND PARTICLE IMPACT

A Thesis

by

NIRMAL SHANKAR SIGAMANI

Submitted to the Office of Graduate Studies of
Texas A&M University
in partial fulfillment of the requirements for the degree of

MASTER OF SCIENCE

Approved by:

Co-Chairs of Committee,	Zoubeida Ounaies
	Ramesh Talreja
Committee Member,	Hung- Jue Sue
Head of Department,	Dimitris C. Lagoudas

May 2010

Major Subject: Aerospace Engineering

ABSTRACT

Characterization of Polyurethane at Multiple Scales for Erosion Mechanisms Under Sand Particle Impact. (May 2010)

Nirmal Shankar Sigamani, B.Tech., Anna University, India

Co-Chairs of Advisory Committee: Dr. Zoubeida Ounaies

Dr. Ramesh Talreja

Thin polyurethane films have been widely used as erosion-resistant coatings on helicopter rotor blades. Published research has mainly focused on empirical studies that relate the mechanical properties such as rebound resilience and hardness of polyurethane to solid particle erosion resistance. However polyurethane possesses phase mixing at multiple scales and thus sand particle erosion resistance depends also on the micro structure and the phase mixing. Hence, it is very important to carry out detailed and systematic investigations to understand the step-by-step mechanism of erosion and how it relates to the polyurethane micro, meso, and macrostructure.

Thermal transitions of the pristine films have been studied through Differential Scanning Calorimetry (DSC) and Dynamic Mechanical Analysis (DMA) yielding micro-scale information such as glass transition temperatures of the hard and soft segments and melting temperature of the soft segment. The next stage of our study involved sand particle erosion tests carried out at 500 mph, at an impact angle of 30°. Test specimens

were exposed to two different sand media at different mass loadings ranging from 0.1 to 20 g/cm^2.

The tools of characterization used on the pristine polyurethane are once again used on the eroded specimens, with the goal to compare pre- and post- erosion results. The comparison of FTIR results on pre-eroded and eroded films reveal the removal of macromolecular bonds corresponding to soft segments in the micro scale. The reduction of the crystalline portion of the soft segment observed from DSC results supports the FTIR findings. Scanning electron microscopy (SEM) images of the eroded specimens are used to correlate the sequence of the damage due to erosion. The observations revealed that after initial ductile deformation of the soft segments on the surface, brittle cracks are formed on the hard segments. The increased exposure to sand particles leads to formation of fragments containing mainly soft segments with cracks in the hard segments propagating in a brittle manner. As exposure increases, cracks intersect and material on the surface gets removed which mainly contains the soft segments as revealed by the FTIR and DSC results.

DEDICATION

To my parents and my brothers

ACKNOWLEDGEMENTS

Everyone who is on the way to achieve their goals has always been supported by a few special people. I too received that kind of support and I am still benefiting from it. First and foremost, I would like to thank my research advisors, Dr. Zoubeida Ounaies and Dr. Ramesh Talreja, for their technical support and the research discussions which helped greatly toward the completion of this thesis. I thank my research committee member, Dr. H .J. Sue for his time and effort in evaluating this research.

I wish to thank all of the group members from the Electro-active Materials Characterization Laboratory (EMCL) for their support in conducting the experiments. This work was made possible due to the financial support of the Texas A&M Aerospace Engineering Department and the Texas Centre for Applied Technologies (TCAT).

I thank Deerfield Urethane, Ltd. and 3M, Ltd. for providing the sample material for the research. I wish to thank Dr. Andrew Phelps, from the University of Dayton Research Institute (UDRI), for his help in conducting sand blasting experiments.

I extend my thanks to my parents and my brothers for being with me in my difficult times. Also I wish to thank my wife, Dhivya Moorthy, and her family for supporting me throughout my master's programme.

NOMENCLATURE

PU	Polyurethane
PS	Polyester
PT	Polyether
T_g	Glass Transition Temperature
T_m	Melting Temperature

TABLE OF CONTENTS

Page

Page

LIST OF FIGURES

Page

Page

Page

LIST OF TABLES

Page

1 INTRODUCTION

1.1 Morphology of Polyurethane

Elastomers are generally co-block polymers with two major segments in which one segment has very low glass transition temperature (T_g) (well below room temperature) whereas the other segment has T_g well above room temperature. Hence, one phase or segment has very flexible nature and the other segment has a rigid crystalline nature. Due to these unique characteristics, the elastomer has more impact absorbing capability without losing the modulus of the material and so it is preferred in the aerospace coating industry. Polyurethane (PU) films and coatings are used to protect the helicopter rotor blades against sand particle erosion such as Blackhawk UH-60, Bell V-22 and Eurocopter SA 315.

Understanding the morphology of PU is important because it has direct implications on the behavior and properties of PU as films or coatings. As mentioned above, PU is a special class of elastomers, named as such due to the presence of a urethane link (see Figure 1.1). The urethane link is generally formed in the linear polyurethanes from diisocyanates and diols, for example, when 1,4-butane diol and hexamethylene diisocyanate are reacted (as shown below):

$$HO(CH_2)_4OH + OCN(CH_2)_6NCO \rightarrow -[O(CH_2)_4OOCNH(CH_2)_6NHCOO]_n-$$

This thesis follows the style of *Macromolecules.*

The result is a PU linear chain as illustrated in Figure 1.2.

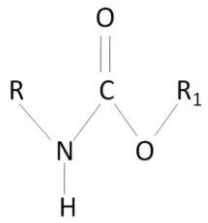

Figure 1.1 Urethane link

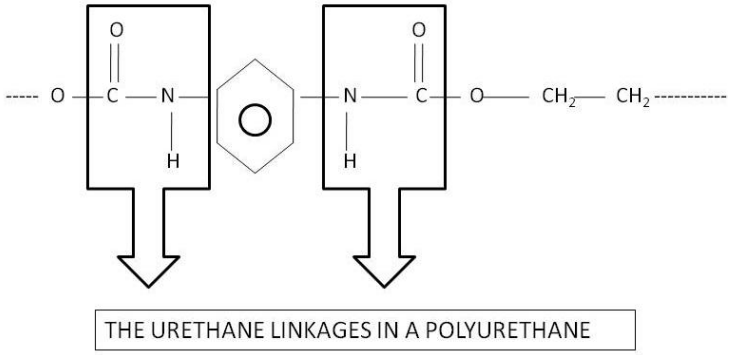

Figure 1.2 Urethane linkages in a PU chain

Figure 1.3 illustrates the arrangement of the basic building blocks of the polyurethane polymer:

1. A is the rigid (or hard) block which determines the network structure of the polymer. A possible chemical composition is diisocyanate.
2. B is the flexible (or soft) block which usually provides the elastic nature of the polyurethane. A possible chemical composition is polyol.

3. C is the chain extender, which can be rigid or flexible, and whose role is to enable chemical cross linking.

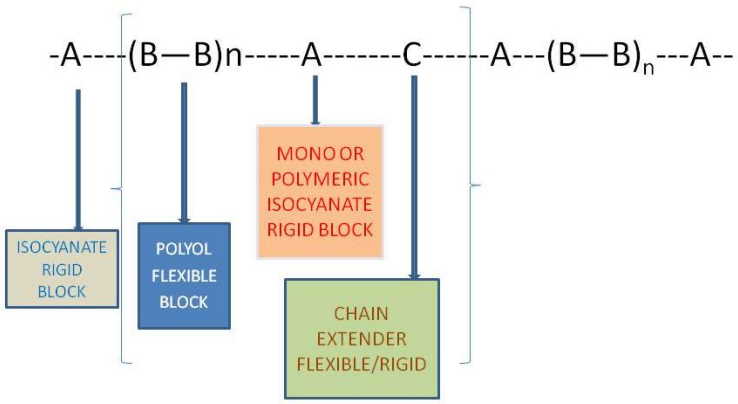

Figure 1.3 Basic unit of PU polymer. Adapted from Hepburn[1]

Figure 1.4 is a schematic of the general steps involved in synthesizing PU. Usually, the flexible block B, a polyol which is either a polyether or polyester, reacts with the hard segment A, a diisocyanate, to form a prepolymer which now contains both flexible and rigid blocks. Further, the excess diisocyanate reacts with either diols or diamines (the chain extender) which lead to a large network with some degree of cross linking. The general arrangement of the flexible and rigid blocks is shown in the Figure 1.5. Generally two transition temperatures occur in polyurethanes, one related to T_g of the flexible blocks and the other related to the dissociation of the inter-chain forces in the rigid blocks, usually above 100°C. Usually by varying the composition of the building blocks, a wide range of strength, stiffness and hardness can be achieved by PU. For

example, the hardness will vary from soft-jelly like nature to hard rigid plastic. Thus, the mechanical properties are strongly affected by the segmented flexibility and chain entanglement of the flexible block (B in Figure 1.3), strong inter-chain forces between the rigid blocks (A in Figure 1.3), and the amount of cross linking enabled by the chain extenders (C in Figure 1.3). The flexible blocks are usually 1000 – 2000 nm long and the rigid blocks are much shorter, usually ~150 nm long.

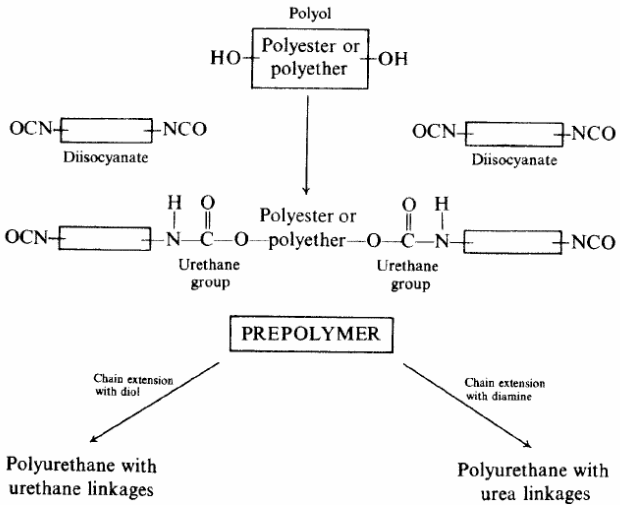

Figure 1.4 Steps for synthesis of PU[1]

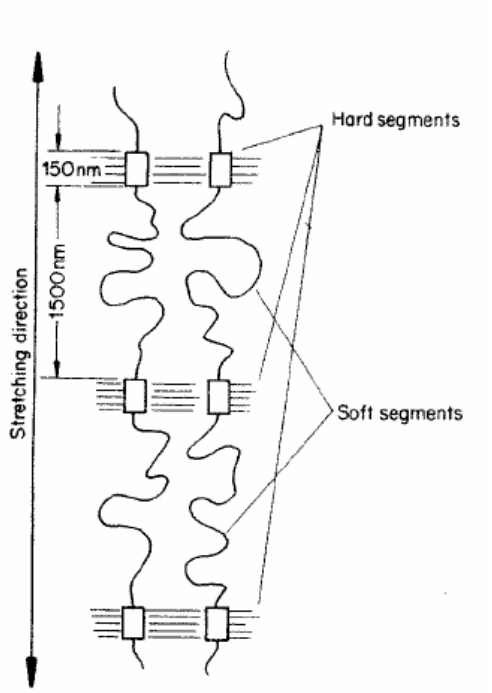

Figure 1.5 Arrangement of hard and soft blocks in PU[1]

It is interesting to note the behavior of the rigid and soft segments in response to mechanical deformation. PU possesses a two-phase structure as noted above, wherein the rigid blocks separate into discrete domains in a matrix of soft blocks. The rigid blocks act as tie down points which are chemically linked with the soft matrix. Figure 1.6a illustrates the structure of PU with the rigid blocks randomly oriented and dispersed in the flexible block matrix. Figure 1.6b demonstrates the orientation of the flexible and rigid blocks in the direction of the elongation when PU is extended by 500%. Upon relaxation, usually flexible blocks disorient, but rigid blocks remain oriented. If the flexible block B is a polyether, crystallization of the flexible blocks occurs when it is stretched to 150% elongation; whereas if B is polyester, crystallization occurs when the

elongation reaches 500% of its original length. Rigid blocks and flexible blocks thus form ordered domains which are held in position by intermolecular forces, mainly hydrogen bonds. This combination of chemical bonds between the rigid and soft blocks, and secondary intermolecular forces between the chains is responsible for the highly rubberlike elastic properties of PU.

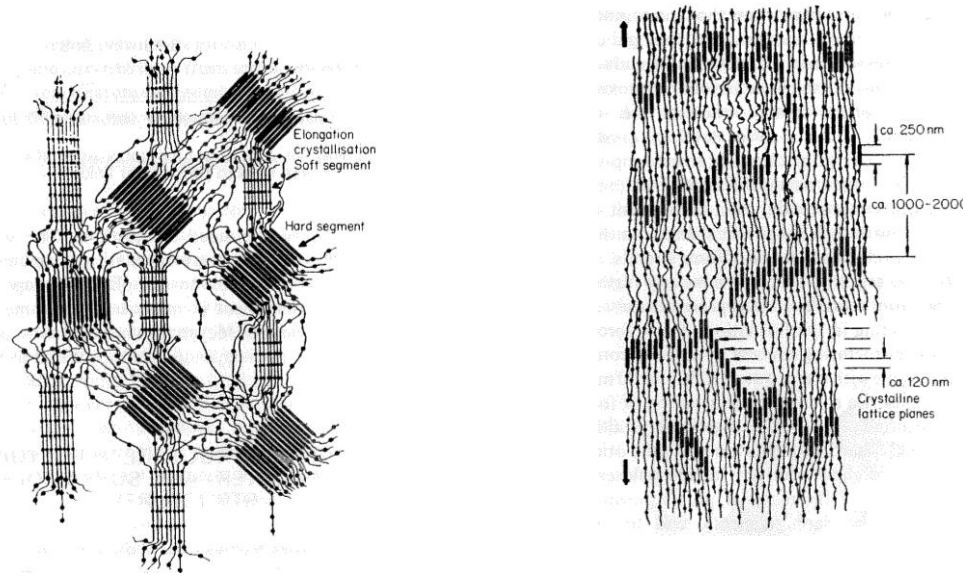

(a) (b)

Figure 1.6 a) Arrangement of flexible and rigid blocks under moderate elongation, and b) Crystallization of flexible and rigid blocks at 500 % elongation[1].

1.1.1 Multi-Phase Separation of Polyurethane

Tocha et al.[2] had used Transmission Electron Microscope (TEM) and Atomic Force Microscope (AFM) to study the multi-phase separation of PU. They proposed that

PU has micro-level and nano-level phase dispersions. The TEM images of the Sample A-701 (Figure 1.7a) which has 30% of hard segment in it shows the micro level dispersion containing globules of 3.8μm diameter and the spherulites. The TEM image of the sample B-501 (Figure 1.7b) which has 50% hard segment in it shows not only globules and spherulites but also some lamellar stack in the micro level.

The AFM images of sample A in Figure 1.8 shows the nano-scale dispersion of the hard segment and soft segment. The globules and spherulites are seen in Figure 1.8a and the nano-scale dispersion in Figure 1.8c.

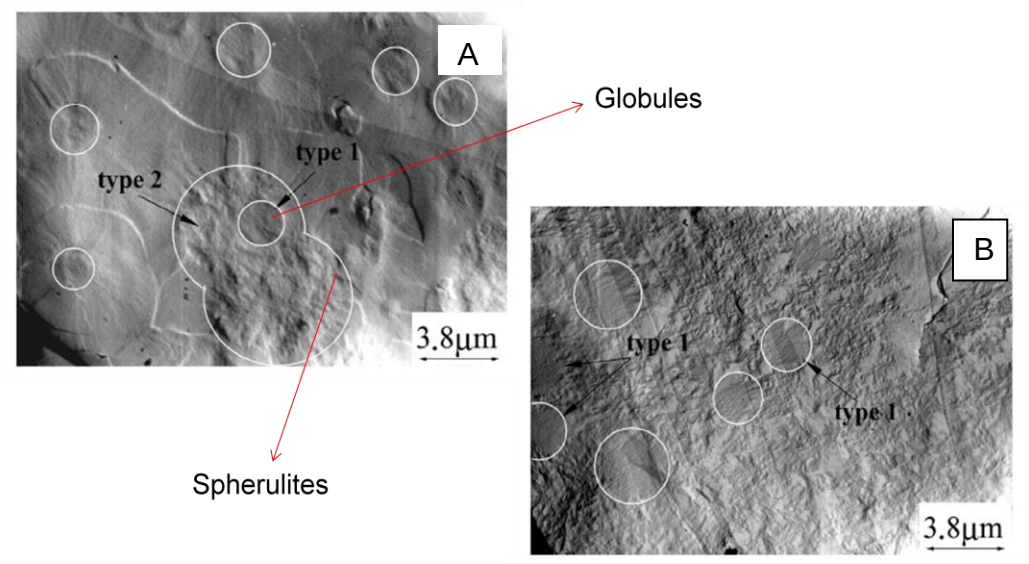

Figure 1.7. TEM images of the micro structure of the samples A (701) & B (501). Adapted from Tocha et al.[2]

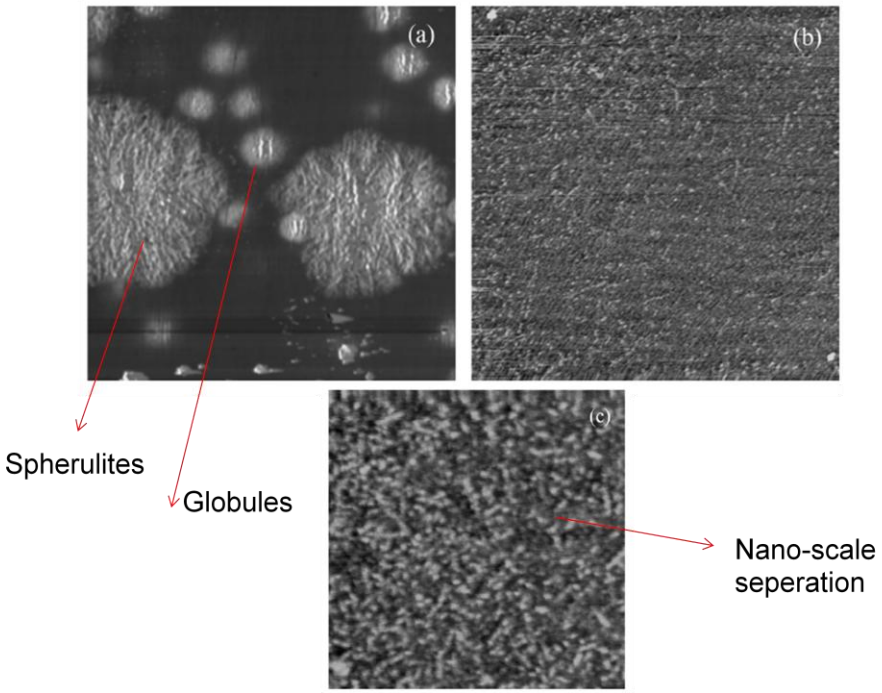

Figure 1.8 AFM images of the nano scale structure of the sample A (701). Adapted from Tocha et al.[2]

The AFM images of Sample B show the lamellar stack (Figure 1.9b) apart from the globules and spherulites (Figure 1.9a). Thus, it is quite evident that the polyurethane possesses multi-scale phase separation. This phase separation is greatly influenced by the composition and the proportion of the hard segment. The schematic shown in the Figure 1.10 illustrates the multi-scale, multi-phase separation in PU. In the micro scale, the soft segment matrix is mixed in the hard segment spherulites whereas in the nano scale the hard segment domains are dispersed in the soft segment matrix.

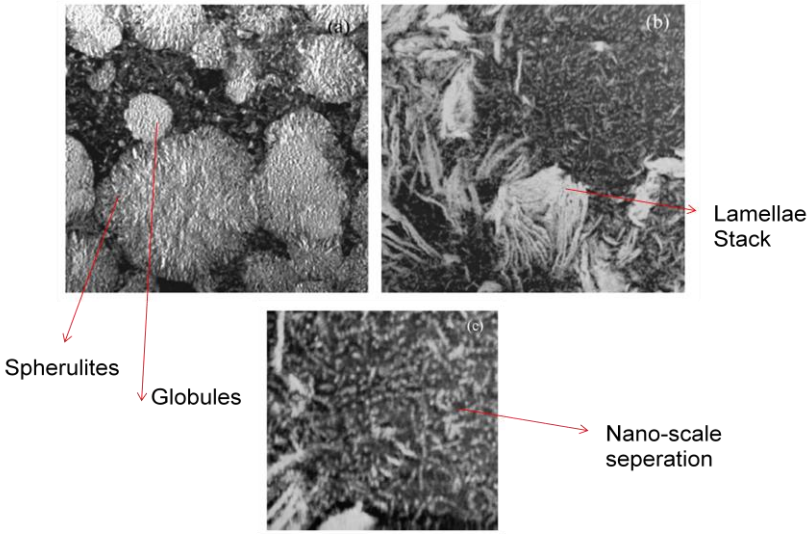

Figure 1.9 AFM images of the nano scale structure of the sample B (501). Adapted from Tocha et al.[2]

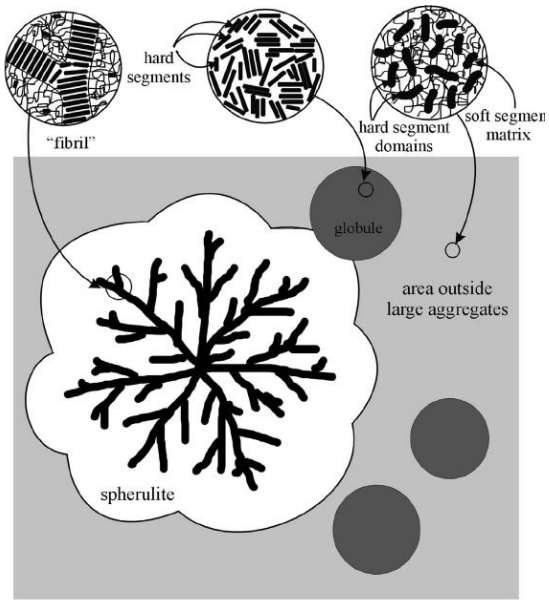

Figure 1.10 Schematic of the micro structure of the polyurethane[2]

1.2 Structure-Property Relationship of Polyurethane

The structure-property relationship in PU is influenced by the nature of the rigid and soft blocks, the amount of chain extenders and percent cross links. For example, rigid blocks in polyurethane polymers partially affect the modulus, hardness and tear strength, and they determine the maximum service temperature by their ability to remain associated at the elevated temperatures. The flexible blocks primarily influence the elastic nature of the polymer and its flow temperature performance, and they make important contribution towards hardness, tear strength and modulus. The contribution of each of the PU segments to its effective properties is detailed in the sections below. A better understanding of this contribution can lead to molecular tailoring of the various units of PU, therefore enabling tuning of its physical properties to particular applications.

1.2.1 Properties of Rigid Blocks

As mentioned earlier, usually rigid segments are formed from diisocyanate. In addition, some chain extenders can also be rigid. Either aromatic diisocyanates such as diphenyl methane diisocyanate (MDI) and toluene diisocyanate (TDI) or aliphatic diisocyanates can be used to form the rigid blocks. Aliphatic diisocyanate are preferred where the high hysteric heat buildup and the discoloration due to light exposure of the aromatic diisocyanates are not desirable. The associated short chain oligomers which usually have high melting points enhance the properties of polyurethane when used as rigid blocks. The choice of the symmetrical, rigid, and bulky molecules as components of the rigid blocks increase the inter-chain forces between the hard blocks. The general properties of the rigid blocks are listed below:

- Inter-chain attractive forces are higher when extensive hydrogen bonding is present
- Short chain nature of rigid segments results in a low molecular weight
- Rigid blocks determine the network structure of PU by cross linking with chain extenders

1.2.2 Properties of Flexible Blocks

Generally, the flexible blocks are polyols and contain either polyesters or polyethers as soft segments. The polyols react with the diisocyanates, the hard segments. Their general properties are listed below:

- Flexible segments usually influence the elastic nature of the polymer
- They usually dominate over and determine the PU properties at low temperatures
- They have very low T_g , usually below room temperature
- They are amorphous and have very low melting points

The ultimate properties of PU depend upon the composition of the polyols. Generally the functionality of the polyols determines the melting temperature of the polyurethanes. Very low melting temperature polymers are formed when simple diols are used to form linear polyurethanes. The physical properties can be categorized based on whether polyesters or polyethers are used as detailed below.

1.2.3 Effects of Polyesters

The polyesters have the tendency to crystallize easily, which leads to strain hardening or cold hardening of the polyurethane elastomers. The advantage of strain hardening is an increase in the tensile strength, however, the elongation at break or ductility decreases as a result. This trade-off can be overcome by using polyesters with highly irregular structure, which has the effect of delaying crystallization to higher elongations. Hence, it is possible to control the mechanical properties of PU by controlling the degree of cold hardening by selecting the appropriate polyester molecular structure. The effect of the polyesters on the properties of PU is shown in Table 1.

1.2.4 Effects of Polyethers

Polyethers have weaker inter-chain interactive forces than polyesters; it follows that the properties of PU based on polyethers will be inferior compared to those of PU made of polyesters. However, the T_g of some of the polyethers confers good performance to the PU; moreover, polyurethane based on polyethers shows better hydrolytic stability than polyesters. Comparison between the effects of polyester and polyether on PU properties are shown in Table 1.

Table 1 Influence of the flexible block on the polyurethane properties[1]

Properties	**PU based on Polyethylene Adipate (Polyester)**	**PU based on Polyoxypropylene Glycol (Polyether)**
Tensile Strength (MPa)	50	29
300 % Modulus (MPa)	38	5
Elongation at Break (%)	650	800
Hardness (IRHD)	88	76

1.2.5 Effect of Size of Rigid and Flexible Blocks

If we increase the molecular weight of flexible block then tensile strength, modulus, hardness and tear strength decreases but increased abrasion resistance is seen. The optimal properties are obtained when the diol/polyester ratio of about 0.4 -2.0 is maintained. Narrow molecular weight distribution for rigid blocks is preferable and it increases modulus, tensile strength and elongation at break due to improved phase separation and formation of domains. Generally, the ratio of diisocyanate/chain extenders decides the size of the rigid block. And if the size of rigid block increases then hardness and modulus increases and elongation at break decreases.

1.2.6 Properties of Chain Extenders

Generally diamines and diols are used as chain extenders. Diamines are capable of introducing urea linkages which forms strong hydrogen bonded interactions and because of this they form polyurethanes with much superior mechanical properties than those which are formed by diols. And in case of diol based polyurethanes, introduction of

additional cross linking is achieved by using triols such as trimethylo propane and it gives better mechanical properties. The increase of triol/diol ratio increases the modulus and resistance to compression.

Generally the rigid segments based on the odd number of carbon atoms reactants form weaker crystalline networks than those based on even number of carbon atom reactants. As shown in the Figure 1.11a, the chain extender with even number of carbon atoms has a symmetry centre. So, the adjacent C = O dipoles lie in opposite directions and it can accommodate four hydrogen bonds easily. In the same way, the chain extender with odd number of carbon atoms has a mirror plane and so the neighboring C = O dipoles lie in same direction. This can accommodate only three strain-free hydrogen bonds as show in Figure 1.11b. So the less intermolecular interaction in odd number of carbon atom based chain extenders prevails and leads to weak network structure. This weaker packing of the rigid block causes the rigid block to be dissolved in the flexible block matrix. Both weaker network and dissolution of hard segment gives very low modulus to the polyurethanes. Consequently, the low modulus lead to greater elongation at break which, in turn, allows further stress crystallization of the flexible polyester segment with consequent development of a higher tensile strength.

Ultimately the tensile strength and elongation at break are higher when the diamine has an odd number of carbon atoms in the chain, 300% modulus and rigid block softening temperature are highest for diamines with even number of carbon atoms. The variation of these properties is shown in the Figure 1.12 a-d.

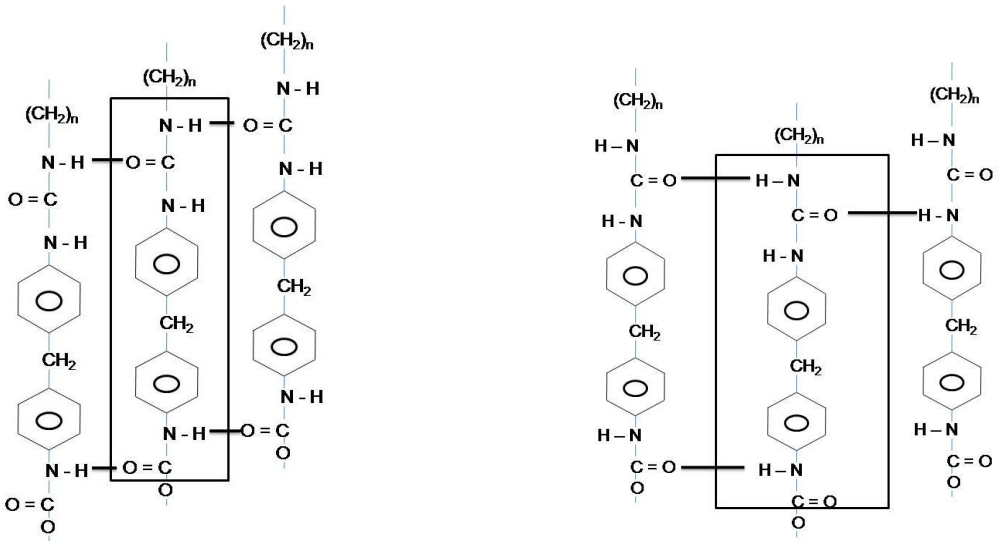

(a) (b)

Figure 1.11 Network structure in PU when the chain extender has a) even number of carbon atoms b) odd number of carbon atoms. Adapted from Born et al.[3]

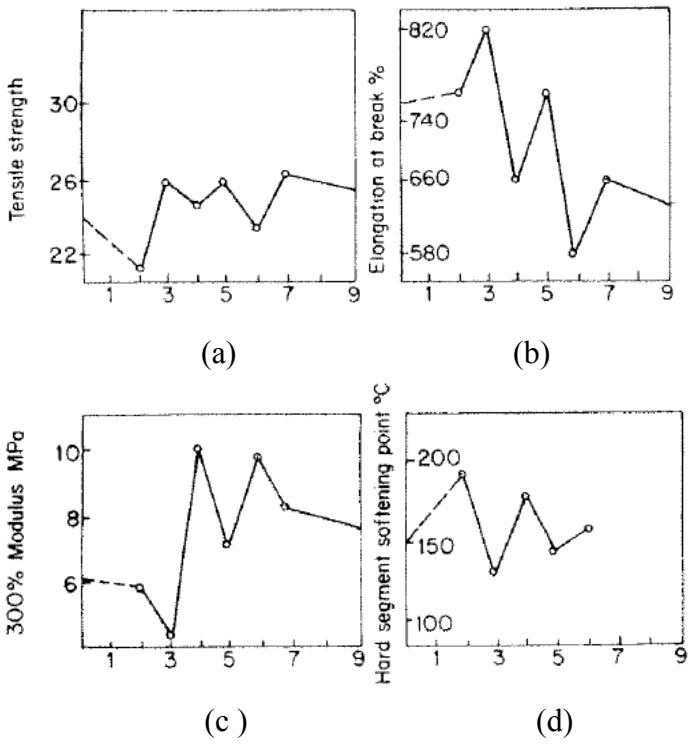

Figure 1.12. The effect of the number of carbon atoms (x-axis) on the properties of polyurethane: a) tensile strength, b) ductility, c) elastic modulus, and d) softening temperature[1]

1.2.7 Effect of Cross linking

In PU elastomers, there are two ways by which cross linking is achieved: through the use of an external trifunctional chain extending agent such as trimethylopropane and through presence of excess diisocyanate which reacts with the urethane and urea groups to give allophanate or biureate linkages

The formation of cross linking is illustrated in Figure 1.13. The degree of cross linking generally influences the mechanical properties of PU. Tensile strength, modulus of elasticity and elongation at break usually increase due to higher chemical cross linking. At first, when the percent cross linking is low, the modulus and tensile strength decrease

as illustrated in Figure 1.14. This downward trend happens due to the existence of the non-covalent intermolecular attractive forces which dominate at low cross linking content. However, as the percent cross linking keeps on increasing, modulus and tensile strength increase again as illustrated in Figure 1.14, and eventually saturate. This behavior occurs because the intermolecular forces lose their effectiveness as increased cross linking causes increased chain separation, and therefore weakening of secondary bonds.

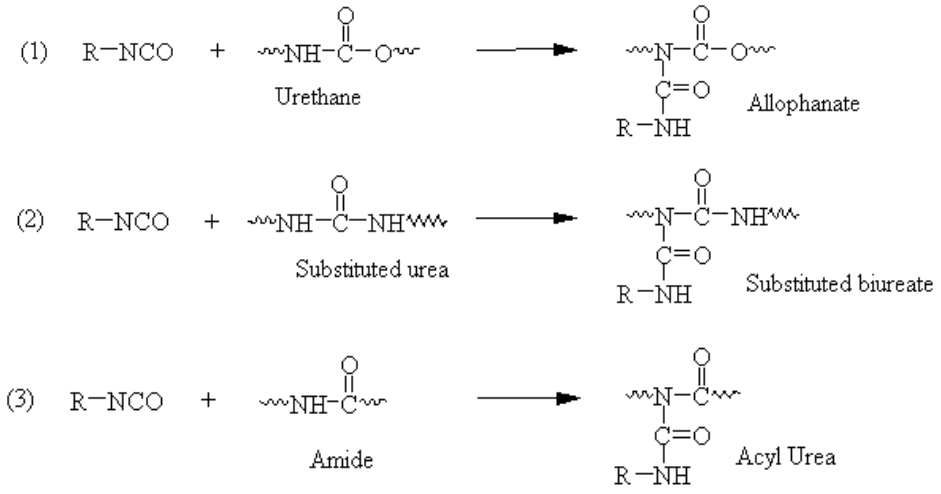

Figure 1.13 The formation of cross linking by excess diisocyanates

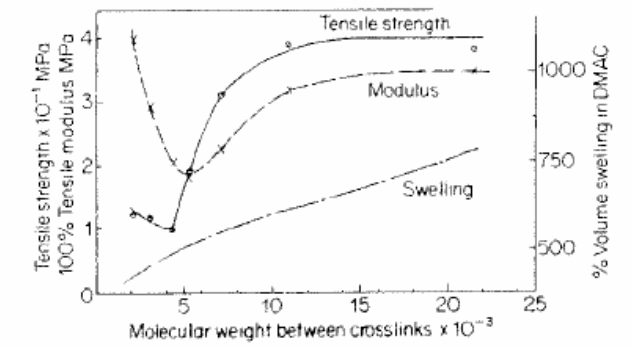

Figure 1.14 The effect of degree of cross linking on the properties of PU[1]

In the region where secondary bonds could dominate, elastomers with strong secondary interactions, like polyester-based urethanes, have physical properties that decrease as percent cross linking increases whereas the properties increase for polyester-based extended diols, which have very weak secondary interactions. Even though some degree of cross linking will help PUs to increase their tensile properties, too much cross linking will disrupt the two phase segregation of the polyurethanes, which lead to undesirable and poor elastic properties.

The effect of cross linking on the modulus of elasticity is represented by the equation,

$$\frac{\sigma}{\gamma} = ARTe^{(\frac{-E_a}{RT})} + (\frac{\nu_C}{V})RT$$

where σ/γ is the stress per unit strain, A is the Arrhenius constant, R is the gas constant, E_a is the activation energy for secondary bonding, v_c/V is the volume fraction of the primary cross links. In the equation, the $ARTe^{(-E/RT)}$ term corresponds to the contribution of the secondary crosslink which were assumed to be related to temperature by the Arrhenius law. At higher degree of cross linking the contribution of the primary crosslink to the modulus decreases and secondary bond is responsible for the higher modulus which is observed on the polyurethane elastomers.

1.3 Sand Particle Erosion

Sand particle erosion is a severe problem in the helicopter blades. There are several methods to evaluate the erosion resistance of the material. Most common method

in use is the sand blasting experiments (Figure 1.15) to simulate the erosion conditions[4]. Measuring the weight loss due to the erosion was the only way to compare the erosion resistance of different materials for better material selection process. There are two major factors that affect the erosion resistance of a particular material. One is the erosion parameters such as impact velocity, impingement angle, mass of the silica and size distribution of the silica. Other is the material parameters such as the material hardness and rebound resilience.

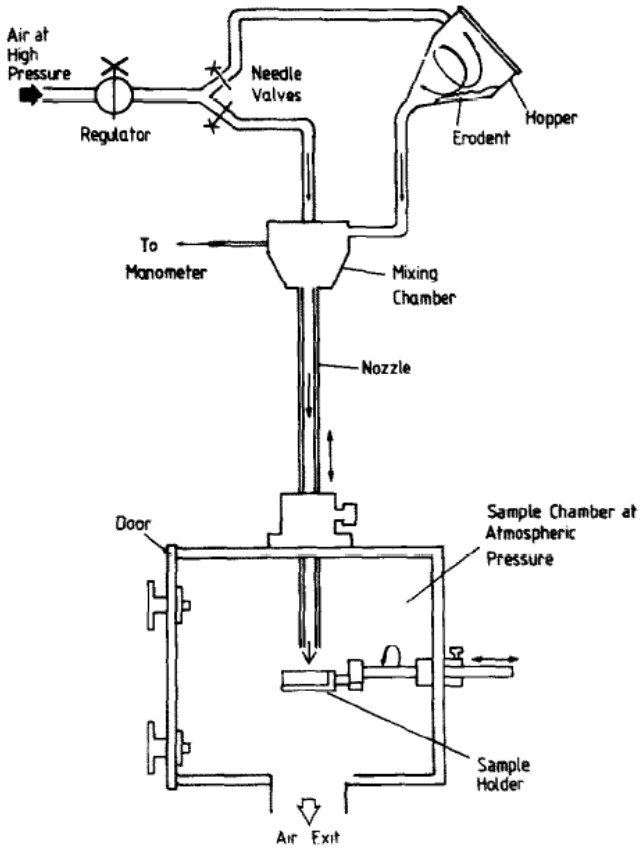

Figure 1.15 Sand blasting chamber experimental setup[4]

1.3.1 Influence of Erosion Parameters

The erosion problem differs from other wear problems in two aspects, one is the range of the impact angle it can incur and the other is the frequency of impact. Abrasion usually happens at very low angles and low impact velocities. But, erosion is capable of much more damage because of higher impact angles and velocities.

1.3.1.1 Impingement Angle

Several studies[4-7] have been carried out for various materials to find out the variation of the erosion resistance with the impingement angle. In metals it was found out that, the ductile materials erode very fast near 20-30° and the brittle materials [5] erode very rapidly near 90° as shown in Figure 1.16. Similar studies were carried for elastomers by Zahavi et al.[6] in which, it was detected that there was variation in the angle at which maximum erosion happens between hard and elastomeric polyurethane coatings. Elastomeric coatings proved to be independent of the impingement angle beyond 45° and further the gain of mass was reported at neat 90° angles as seen in Figure 1.17. This may be due to the silica particles getting embedded in to the coatings at normal angles of impact.

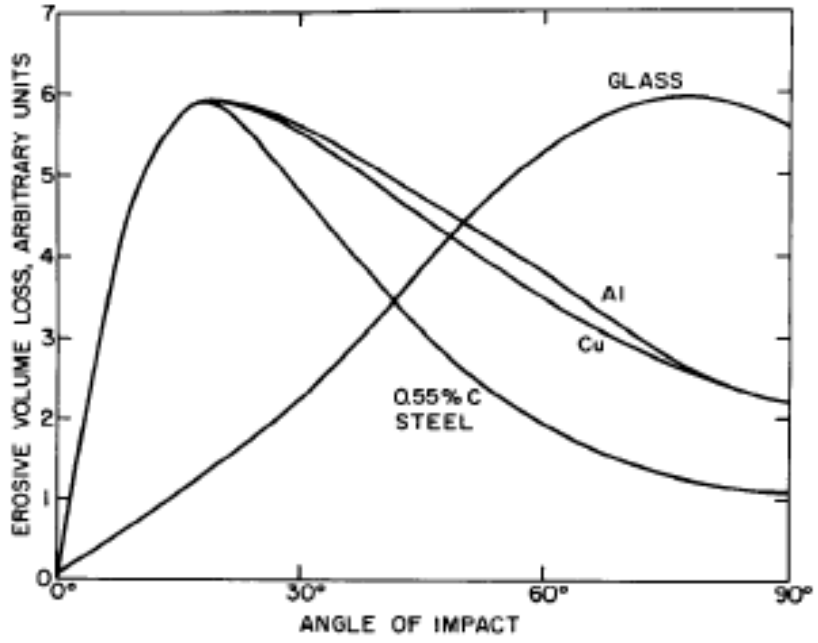

Figure 1.16 Variation of the erosion resistance with impingement angle in metals[5]

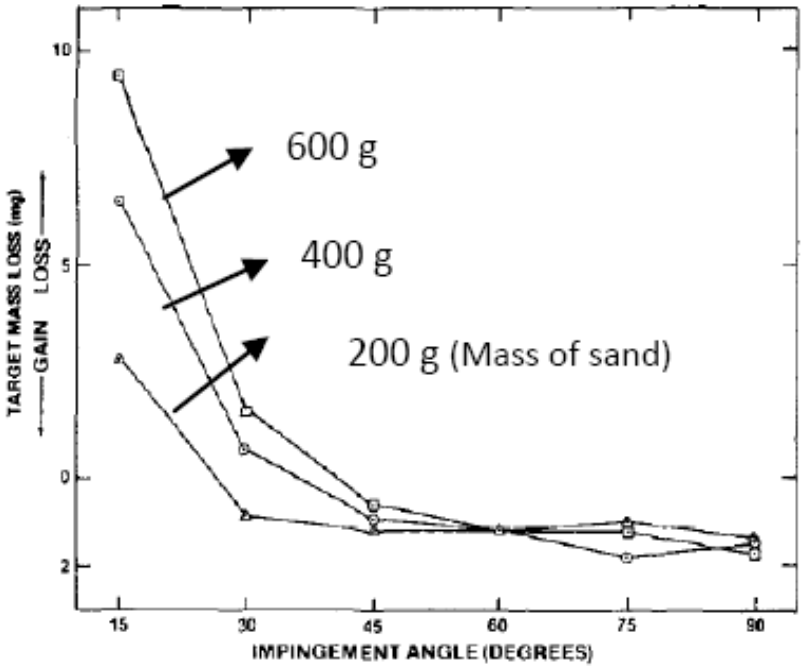

Figure 1.17 Variation of the erosion resistance with impingement angle in elastomeric polyurethane coating[6]

1.3.1.2 Impact Velocity

The sand particle erosion varied drastically with the increase in the impact velocity. And there exists a threshold velocity for particular material above which the erosion rate will be multifold. Arnold et al.[7] studied the effect of impact velocity on the solid particle erosion observed that the erosion rate was less and the distribution of the erosion was uniform when the impact velocity was less than 60m/s as shown in Figure 1.18. But once, the velocity exceeded this range, the high erosion rate was observed and the formation of the local deep pits was also seen as shown in Figure 1.19. Moreover, the impact velocity of the sand particle and the distribution of the sand particle in the air media determine the frequency of impact of the sand particle on the coatings.

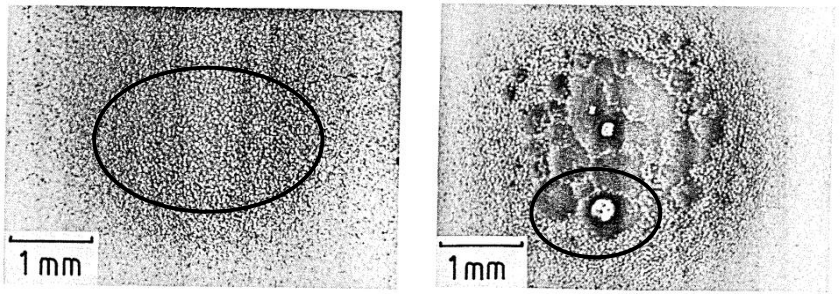

(a) (b)

Figure 1.18 SEM micrograph of the surface of the natural rubber at 90° impingement angle and impact velocity a) 60 ms^{-1} b) 90 ms^{-1} [Adapted from Arnold et al.[7]]

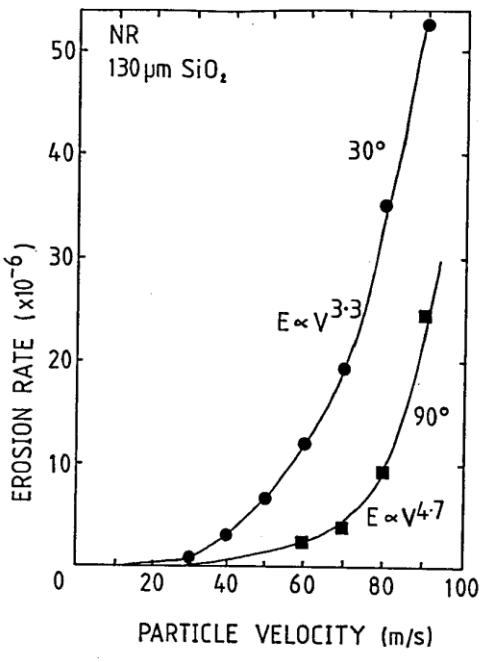

Figure 1.19 Variation of the erosion rate with the impact velocity[7]

1.3.1.3 Mass and Size of the Silica

The total mass of the silica impinging on the specimen is generally controlled by the exposure time of the specimen to the sand particle impact with a constant mass flow rate. Thus, the level of exposure of this specimen can be used as a method to simulate different stages of sand particle erosion in the films and coatings. Size and shape of the silica particles may vary between sharp angular particles to smooth round shaped particles. Generally, the sharp angular silica particles (240-550 μm) impart more damage by roughening the surface of the films heavily.

1.3.2 Influence of Material Parameters

For a given erosion parameters, different material exert different level of erosion resistance which primarily depend on the material parameters such as Hardness and Rebound resilience. Researchers [4,8] had studied the effect of these material parameters on erosion resistance.

1.3.2.1 Effect of Rebound Resilience

Rebound resilience is the ratio of the energy which can be restored immediately to the total energy supplied. It can be found out by the ball-drop method. A steel ball of 6.35mm diameter is dropped on the thick samples of the elastomers and rebound resilience is the ratio between the height of the rebound and the height of fall. Hutchings et al.[8] carried out erosion experiments with the elastomers having different rebound resilience values to study the effect on erosion resistance. Figure 1.20 shows that the high resilient elastomers are very effective for erosion resistance. They also found that the rate of erosion varied exponentially with the rebound resilience as shown in the Figure 1.21.

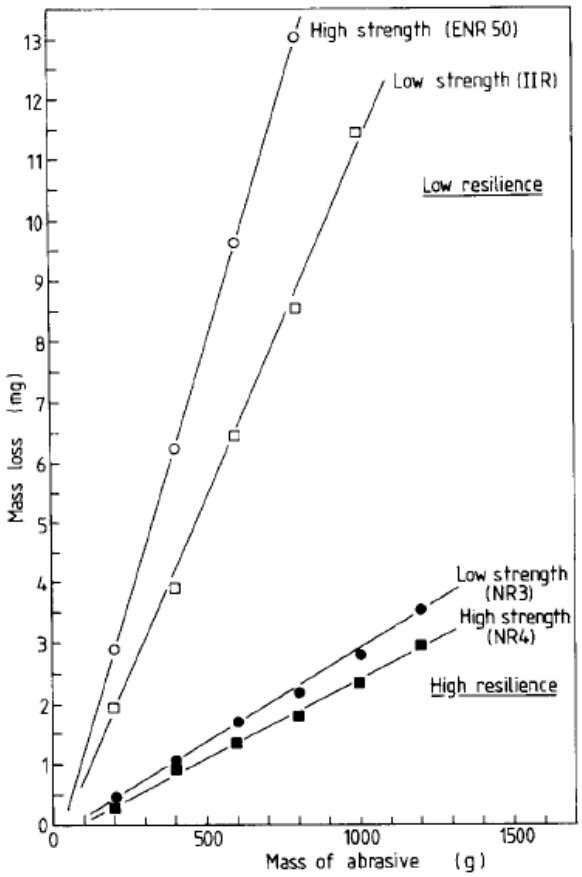

Figure 1.20 Effect of rebound resilience on erosion resistance[4]

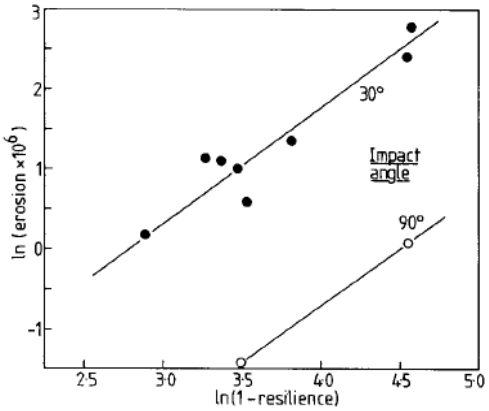

Figure 1.21 Relation between rebound resilience and erosion resistance[4]

1.3.2.2 Effect of Hardness

Hardness of the elastomers which depend on the amount of the hard segment percentage in the material is a vital parameter which can change the mechanism of erosion. Hutchings et al.[8] studied the effect on erosion resistance of the mechanical properties of polyurethane. By keeping the rebound resilience values essentially constant, they studied the variation of the erosion resistance with respect to the variation of the hardness, tensile strength and elastic modulus. Figure 1.22 shows that the higher the hardness, higher the erosion rate. Hard elastomers had very high recovery time and had high erosion rate as shown in Figure 1.23.

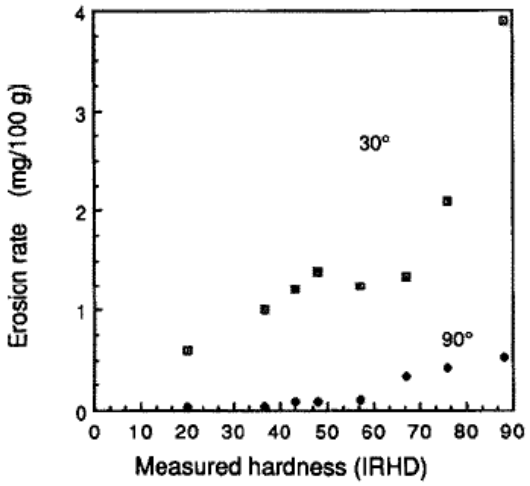

Figure 1.22 Effect of hardness on the erosion rate[8]

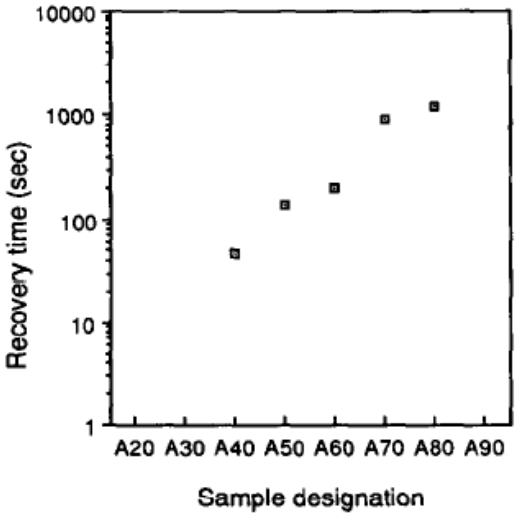

Figure 1.23 Relation between hardness and the recovery time[8]

1.3.3 Mechanisms of Erosion

The understanding of the mechanism of erosion is very much required in order to progress in the optimization of the materials used currently for erosion resistance. Arnold et al.[7] studied the mechanism of material removal in two unfilled elastomers and explained that there exists a incubation period during which the impact energy imparted from the sand particle impingement is mainly used for roughening the surface. After this, incubation period, the steady state erosion happens and the material removal occurs by the formation of cracks.

Zahavi et al.[6] explored more about the mechanism of erosion in polyurethane coatings and found that the propagation of fine cracks from surface in to the bulk leads to the formation of fragments. Mechanism of erosion is better understood with the consideration of the recovery time. Hard elastomers have higher recovery time and takes longer time to dissipate the energy absorbed. Hence, when the sand particle impacts the

region which has not yet fully recovered, then the repeated cyclic impact on that region eventually causes plastic deformation and eventually the material is removed locally.

Consequently, it is believed that the solid particle erosion in the polyurethane occurs in four stages. Initially, the surface cracks are formed by the cyclic impact loading and the cracks tend to propagate by the impact of the sand particles on the existing cracks. The cracks tend to travel both on the surface and also in to the bulk. Then, when the propagating cracks intersect each other, the local material is chipped out of the surface and forms fragments. Finally, under steady state erosion, the fragments are removed from the surface causing mass loss of the material. Figure 1.24 shows the schematic of the four stages of the material removal during the solid particle erosion.

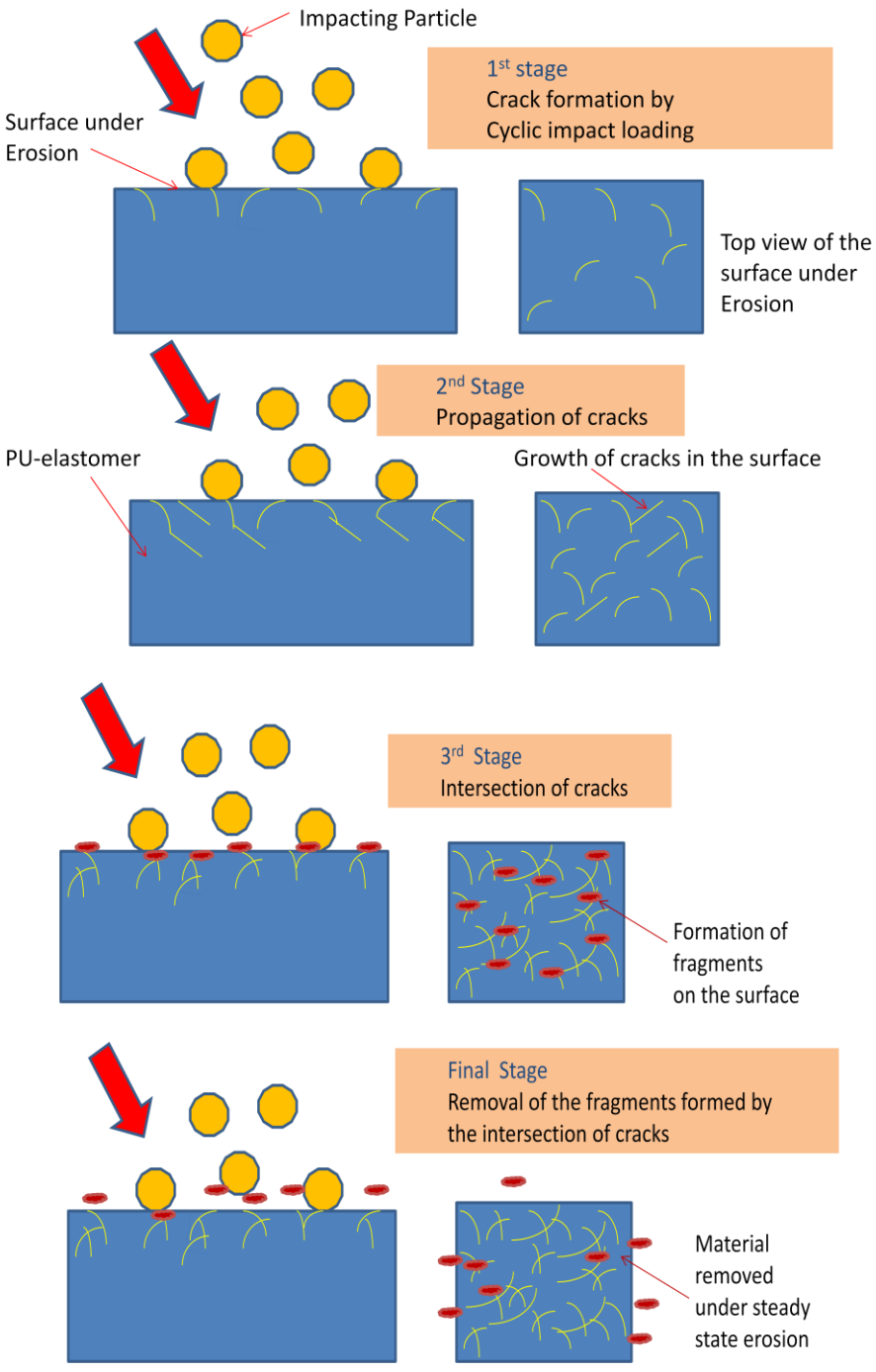

Figure 1.24 Mechanism of material removal during the erosion of polyurethane

1.4 Problem Statement

The preceding sections have reviewed the three major areas of interest, namely, morphology of PU, sand particle erosion parameters and current understanding of the mechanism of material removal. The erosion resistance of the polyurethane had been approached up to now with a main focus on empirical studies that assess the effect of cross linking density and hardness of polyurethane on solid particle erosion resistance. Also, several studies had been done to better understand the morphology and phase separation of PU. Given the unique multi-phase structure of PU, it is important to investigate sand particle erosion at multiple scales, rather than just focus on mass loss of material as it has been done so far in the literature. Proper understanding of the micro structural changes due to the erosion is crucial to address the unresolved problems in the aerospace design and the maintenance field.

This research focuses mainly on the systematic investigations of the mechanism of sand particle erosion in PU films, and the influence of micro structural changes at different stages of erosion. The effect of morphology of PU is assessed both by considering PU films of different hardness values (and hence different % HS) and by investigating two types of PU: a polyester- and a polyether- based PU .

Initially, the pre-erosion samples are characterized using different techniques such as DSC, DMA, FTIR, nano-indentation. Then some of these characterization techniques are repeated for samples post-erosion, The strategy is to analyze the results from various characterization techniques to develop an understanding of erosion mechanism at various scales: from bond level and micro structure to macro level.

1.5 Organization of Sections

This study on the characterization of polyurethane at multiple scales for erosion mechanisms under sand particle impact has been organized into four sections. Section 1 covers the literature review of the problem by introducing earlier approaches used to study erosion in PU. The morphology and phase separation of the polyurethane material are also discussed. Finally, the mechanism of material removal due to sand particle erosion as understood so far in the literature is outlined.

Section 2 introduces the experimental approach of this study by describing the techniques used to characterize the pristine films such as Differential Scanning Calorimetry (DSC), Dynamic Mechanical Analysis (DMA), Fourier Transform Infrared Spectroscopy (FTIR) and Scanning Electron Microscopy (SEM). The sand blasting chamber experimental setup and the details of the test conditions are presented. Finally, the approach used to evaluate the micro structural changes in polyurethane using these techniques is also discussed. Section 3 analyzes the results obtained from the DSC, DMA, FTIR and SEM on both the pristine and the eroded films. In addition, the progress of damage at different stages of erosion is thoroughly studied using the SEM images. Finally, an attempt is made to correlate the experimental findings to the micro structural changes. Section 4 summarizes important findings, concludes this research and discusses the future follow-up work to be carried out.

2 EXPERIMENTS

2.1 Experimental Material

Thin polyurethane films with thickness ranging from 0.3-0.5 mm were supplied by Deerfield Urethane Ltd and 3M Ltd for this research. The films are pure thermoplastic elastomers with no additives. Four cases, of which two were polyester based and two were polyether based PU films, are considered for this study. The hardness of the films varied between 80 Shore A to 90 Shore A ensuring there is enough variation in the micro structure in the films under study. The two polyester based PU films are named as PS-80 & PS- 85, showing both chemical composition (PS for polyester) and the hardness (the number value). Similarly, the two polyether based PU are named as PT-82 & PT-90.The mechanical properties of the films are given in Table 2.

Table 2 Mechanical properties of the polyurethane samples

Properties	**PS-80**	**PS-85**	**PT-82**	**PT-90**
Type	Aliphatic Polyester	Aromatic Polyester	Aromatic Polyether	Aromatic Polyether
Hardness (Shore A)	80	85	82	90
Ultimate Tensile Strength (MPa)	35.02	68.94	61.36	66.87

2.2 Characterization of Pristine Films

The four different PU samples are initially studied using DSC, DMA and FTIR in order to understand more about its structure property relationships. These tools are also used to observe the phase separation of the PU samples. As we have discussed earlier, these four different cases represent two major types of PU, polyether and polyester, with additional variation in the micro structure. The variation in the micro structure is expected to result from the variation in the amount of the hard segments. Shore A hardness usually represents the hard segment percentage approximately. Higher the hard segment percentage, higher the hardness owing to the more rigid blocks in the micro structure. The two main objectives of the characterization are to understand the property changes owing to micro structure and to explore the capability of these tools to assess the micro structural changes.

2.2.1 Thermal Transitions

PU has two different segments and has many thermal transitions which significantly change the mechanical behavior of the material. The main thermal transitions are listed below:

1. T_g of the soft segment
2. T_g of the hard segment
3. T_m of the soft segment
4. T_m of the hard segment

Among these, the glass transition temperatures are more significant as it falls near the operating temperature range of the material. Hence, the samples were studied using

DSC and DMA to know the thermal transition temperatures of them and the variation of them with both the type of the PU and the hardness.

Apart from revealing the transition temperatures, DSC results can reveal more information about the phase separation of the PU also. Based on the composition of diisocyanates, percentage of hard segment, hard segment crystallinity and the dispersion of the hard segments in the soft segments, the thermal transition varied for polyurethanes. Spathis et al.[9] studied the thermal behavior of the polyurethane using DSC, and found that the melt endotherm of the soft segment varied for different NCO/OH ratio (Figure 2.1). NCO represents the urethane link in hard segment and the OH represents the polyols in the soft segment and hence the NCO/OH ratio generally represents the amount of cross linking. The soft segment melt endotherm does not exist for very high NCO/OH ratio, because the more crosslink points prevent the free flow of the soft segments to melt. From the melt endotherm, the soft segment crystallinity can be calculated. The extent of the peak of the endotherm gives information about the phase separation of the hard/soft segments.

The dispersion of the hard segments in the soft segment also changes the T_g of soft segment. If the hard segment is well dispersed, then it would hamper the movement of the soft segment molecules eventually increasing the T_g of the soft segment. Lee et al.[10] studied the effect of the different isocyanates on the micro structure of the polyurethanes. When compared with the thermal transition of the polyurethane without chain extenders, it was observed that some of the diisocyanates changes the T_g of the soft segment while others do not. This feature is directly related to the miscibility of the hard

segment and the soft segment. Hence, by the thermal transitions of the PU, the changes in the micro structure can be understood. Thus the study of the thermal transitions using DSC proves to be a much capable approach to find out the properties that relate directly to the micro structure. The different thermal transitions shown by the different diisocyanates are shown in the figure 2.2b. The thermal transitions of PU without chain extenders are shown in figure 2.2a.

Similarly Dynamic Mechanical Analysis (DMA) can reveal significant details about the structure property relationships of PU films. Visco-elastic properties such as storage modulus, loss modulus, tan δ & rubbery plateau modulus are obtained as functions of time, frequency and temperature. The tan δ value will give the amount of visco-elastic damping of the polyurethane elastomer which depends primarily on the cross link density. The cross link density in PU can significantly change the micro structure by the formation of more rigid blocks and eventually increasing the rubber plateau modulus. The DMA experiments are done for our PU film samples to know the variation of its dynamic properties between them.

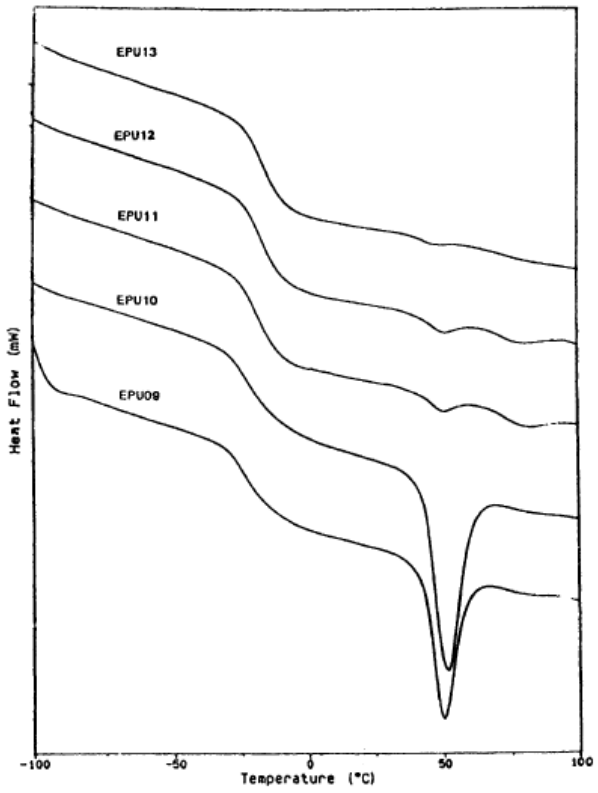

Figure 2.1 Effect of NCO/OH ratio on the thermal behaviors of PU[9]

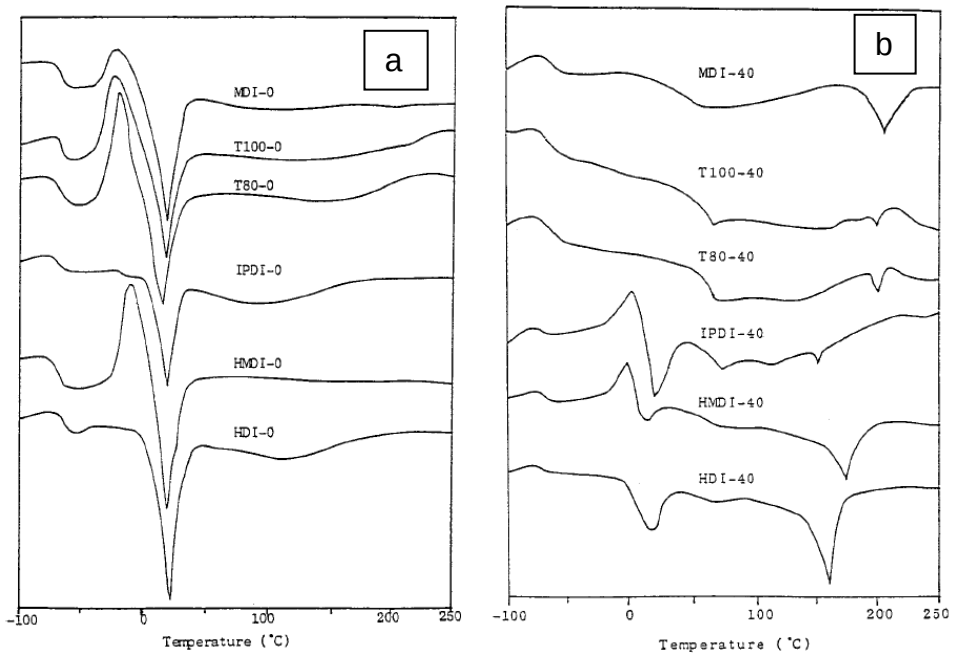

Figure 2.2 The effect of different diisocyanates on the DSC results[10]

2.2.2 Fourier Transform Infrared Spectroscopy (FTIR)

Using this tool, the composition of the hard and soft segment mixtures in elastomers can be observed. Using this spectroscopy we can characterize different hydrogen bonds formed and the phase segregated structure of the polyurethanes. Each molecular bond has a unique frequency on the FTIR spectrum. Thus, the existence of certain bonds can be easily identified. In the polyurethane N=H and the C=O are the significant bonds which represent the urethane and the carbonyl linkages. Moreover, the free N=H and the N=H bonded with C=O would have different frequencies in the spectrum. Hence, the amount of the free N=H gives the information about the amount of the cross linking present and the frequency shift from the free N=H bond and the bonded

N=H gives the strength of the bond. Similarly, the C=O bond gives details about the portion of the C=O in the urethane linkage as well as the free C=O bond. Thus, FTIR is very effective tool for studying the composition of the polyurethane especially the molecular bonds.

Spathis et al.[9] studied the effect of NCO/OH ratio on the phase separation of the polyurethanes using FTIR by keeping the constant hard segment percentage. The frequency shift between the bonded N-H group (ν_b) and the free N-H group (ν_f) directly gives the measure of the strength of the hydrogen bond between N-H---C=O.

$$\Delta\nu = \nu_b - \nu_f$$

If the strength of hydrogen bond increases then the distance between the N=H---C=O decreases and it results in the shift in the frequency between ν_b and ν_f.

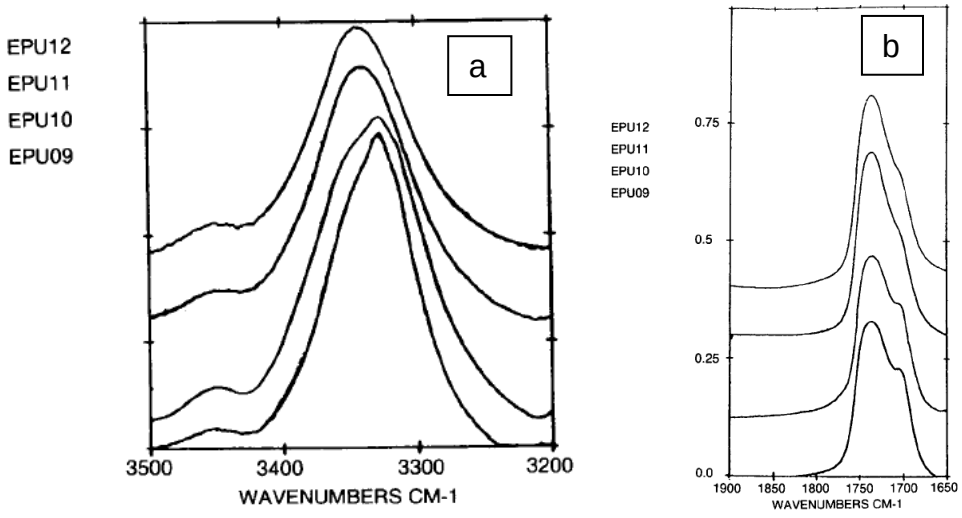

Figure 2.3 Effect of NCO/OH ratio on the chemical bonds of polyurethane[9]

In Figure 2.3a, the EPU09 & EPU10, which are thermoplastic polyurethanes, show asymmetric and broad peaks whereas the EPU 11 and EPU 12, which are

elastomeric, show sharp and symmetric peaks. The frequency shift of the free and bonded N-H for the first group is 123 cm^{-1} and for the second one it is 109 cm^{-1}. Thus, the nature of the change in the cross link between the thermoplastic and elastomeric PU has changed the frequency shift. Similarly, in Figure 2.3b in the C=O bond region, the thermoplastic PU shows the weak shoulder at 1700 cm^{-1} corresponding to the hydrogen bonded urethane carbonyls. As the NCO/OH ratio increases, the intensity of the peak varies.

Thus, using FTIR the existence of the particular bonds which represent the two different types of the PU segments and the amount of the cross linking between them can be studied. The FTIR experiments are done for our samples to know the variation in the molecular level due to the change in the micro structure.

2.3 Sand Blasting Experiment

The PU thin films were subjected to sand blasting under simulated erosion conditions at University of Dayton Research Institute. The experimental setup is shown in the Figure 2.4. The experimental setup contains three major systems[11]. The sand blasting system contains the air compressor with ejector nozzle, controlled sand media delivery system and the dust collector system. The compressed air is mixed with the silica particles flowing out from the sand media delivery system and it flows out of the ejector nozzle with constant velocity. Second system is the high velocity measurement system in which generally the laser Doppler velocimeter is used to control the impact velocity at a constant rate. Another system is the transition motor controller system and the sample holder. The sample holder containing 16 samples is seen in the Figure 2.5.

The frontal mask ensures the exposure of the sand particle is restricted to the desired area of the samples.

The PU films under study were exposed to impact velocity of 500 mph and impact angle of 30º. Generally desired impact angle is obtained by the rotation of the sample holder with respect to the ejector nozzle. Two different types of sand particles were used for sand blasting: Gulf sand (240-550 μm) and round sand (177-250 μm). The films were subjected to different stages of erosion by varying the mass of the silica particles impacting on the surface of the film. The different level of exposure is obtained by varying the exposure time of the sample to the sand particles by keeping the constant flow rate. Thus, the four different samples of PU films were subjected to five different mass loadings 0.5, 1.0, 2.0, 10.0 & 20.0 g/cm^2. Tables 3 and 4 give details about the total number of experiments and the experimental parameters.

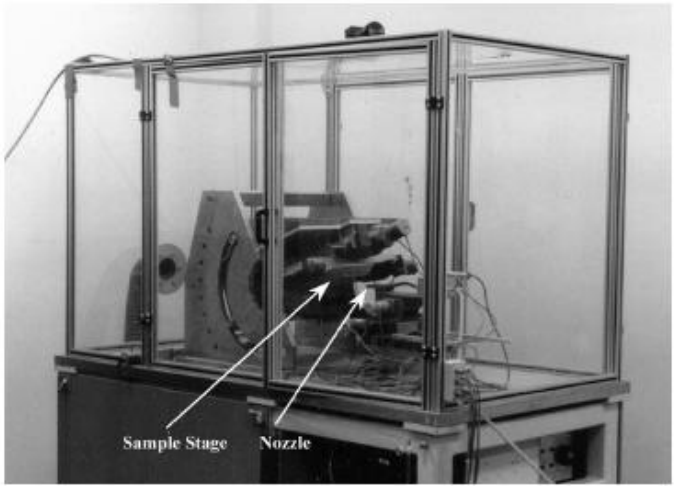

Figure 2.4 Sand blasting experimental setup at UDRI, Dayton[11]

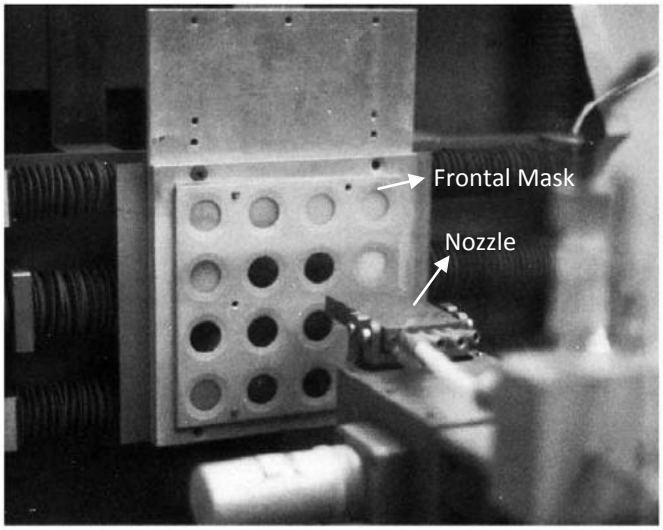

Figure 2.5 Frontal mask showing the fixture containing specimen[11]

Table 3 Plan of tests for 5 different mass loadings with round media

Tests	**Test-1**	**Test-2**	**Test-3**	**Test-4**	**Test-5**
Media	Round sand (177-250 µm)	Round sand (177-250 µm)	Round sand (177-250 µm)	Round sand (177-250 µm)	Round sand (177-250 µm)
Impact Velocity (MPH)	500	500	500	500	500
Impingement Angle (°)	30	30	30	30	30
Mass Loading (g/cm^2)	0.5	1.0	2.0	10.0	20.0

Table 4 Plan of tests for 5 different mass loadings with angular media

Tests	**Test-6**	**Test-7**	**Test-8**	**Test-9**	**Test-10**
Media	Gulf sand (240-550 µm)	Gulf sand (240-550 µm)	Gulf sand (240-550 µm)	Gulf sand (240-550 µm)	Gulf sand (240-550 µm)
Impact Velocity (MPH)	500	500	500	500	500
Impingement Angle (°)	30	30	30	30	30
Mass Loading (g/cm^2)	0.5	1.0	2.0	10.0	20.0

2.4 Post Erosion Characterization of PU Films

The tools of characterization used on the pristine polyurethane are once again used on the eroded specimens, with the goal to compare pre- and post- erosion findings, relate them to the extent of damage, and deduce the mechanism responsible for the change at both the meso as well as micro scales. By using these experiments and observations, an attempt is made to explore the link between the mechanism of erosion and the micro structure of the polyurethane.

FTIR and DSC results of the pristine and damaged films will be compared to analyze the extent of damage on the surface of the PU films. By observing the results from these techniques on the films exposed to different level of damage, the trend in the corresponding damage in micro structure will be detected. The melting peak of the eroded films using DSC will be analyzed for any possible reduction which can reveal the removal of the soft/hard segments. N-H and C=O bonds corresponding to the hard and soft segments respectively will be investigated using FTIR on the eroded films to detect the destruction of the bonds. SEM of the eroded surface will be conducted to observe some trend in the progress of the damage. The variation of the trend will be correlated with the different type of polyurethane used. Finally the SEM of the cross sectional view of the eroded films will be done to detect the progression of the damage into the bulk. The experimental approach of the characterization of the PU films for sand particle erosion is shown in Figure 2.6.

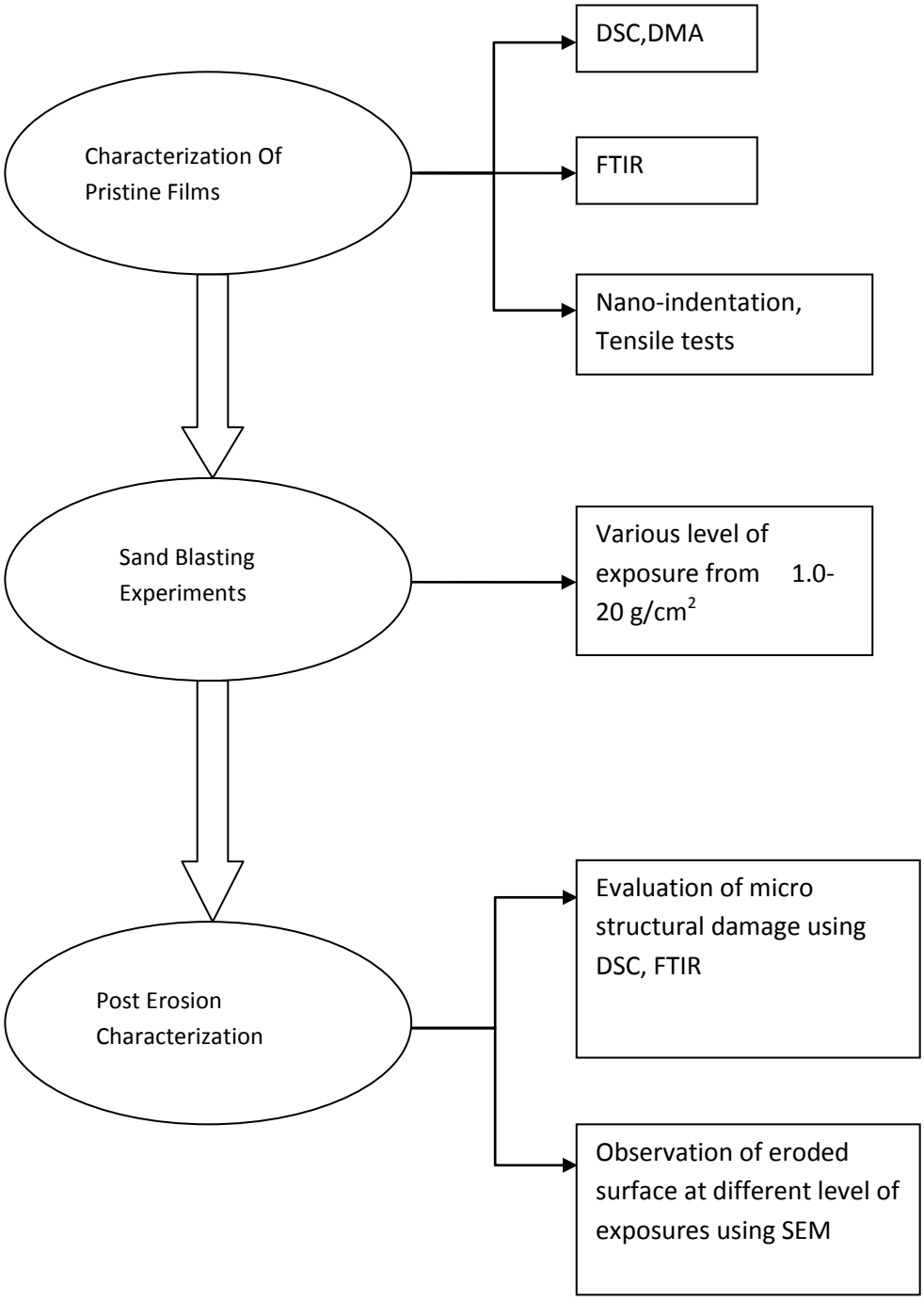

Figure 2.6 Flow chart of the experimental approach

3 RESULTS AND DISCUSSIONS

3.1 Characterization of Pristine Films

3.1.1 Differential Scanning Calorimetry (DSC)

The thermal behavior of the pure thermoplastic polyurethanes PS-80, PS-85, PT-82 and PT-90 is found by using DSC. The DSC experiment was done from the temperature range of -90°C to 170°C. The temperature increment rate of 10°C per minute was taken. Two cycles of the temperature run were done in order to avoid any transitions due to its processing oriented morphology changes. Figure 3.1 shows the thermal transitions captured by DSC for all the PU films. From the results, it was found that in all the three PU-films, apart from the T_g of soft segment around -50°C , another glass transition was seen near 70°C and this was found only in the first cycle.

Woo et al. [12] have showed that the thermal transition can occur in polyurethane due to the disassociation of hydrogen bonds between the secondary amine in the urethane and the ether. And there may be a possibility that a thermal transition may occur due to the inter-domain phenomenon of annealing induced ordering. Hence, it is believed that this transition around 70°C which is observed only during the first cycle, is due to some processing oriented order of the crystal structure of the hard segment.

It is noted from Figure 3.1 that the Glass transition temperature of the soft segments varied with respect to the hardness. For the films with higher hardness, the higher amount of hard segments shifts the T_g considerably.

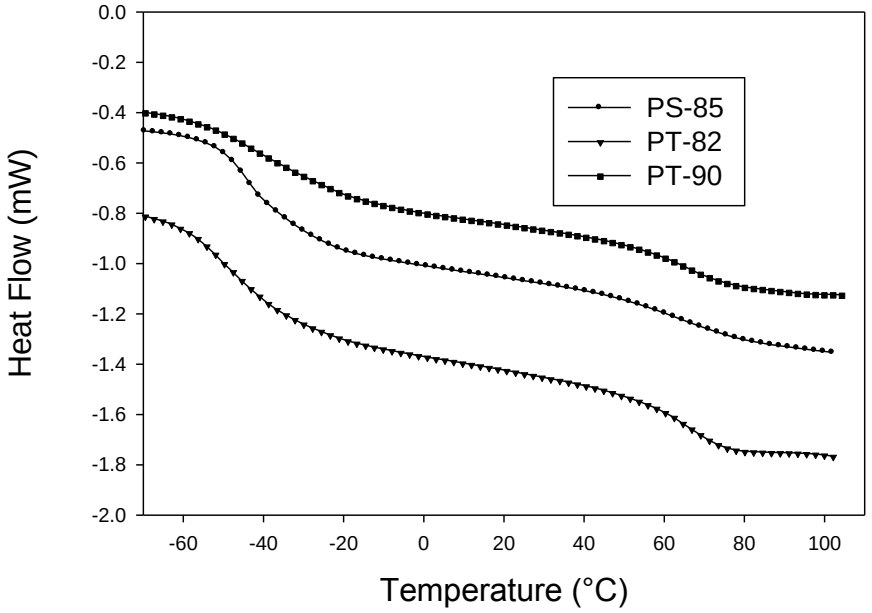

Figure 3.1. Thermal transitions of the PU films observed using DSC

3.1.2 Dynamic Mechanical Analysis (DMA)

The DMA experiments were carried out for the PU films. The glass transition temperature obtained from DMA was very close to the DSC experiment results.

The tan-δ peak corresponding to glass transition in DMA experiment gives us more details about the morphology. The composition of the PU greatly affects the T_g of Soft segment. Apart from that the shape of the peak also changes corresponding to the change in the phase mixing in the micro structure as observed in Figure 3.2. The low hardness films PT-82 & PS-85 show a sharp Tan-δ peak corresponding to the glass transition where as the PT-90 shows a broad peak because of the mixing of the phase between soft and hard segments. In Figure 3.3 the thermal transition is observed with a slight slump in the Storage modulus, around 70°C for all the samples. This is related to

the thermal transition corresponding to the annealing induced crystal structure arrangement of the hard segment.

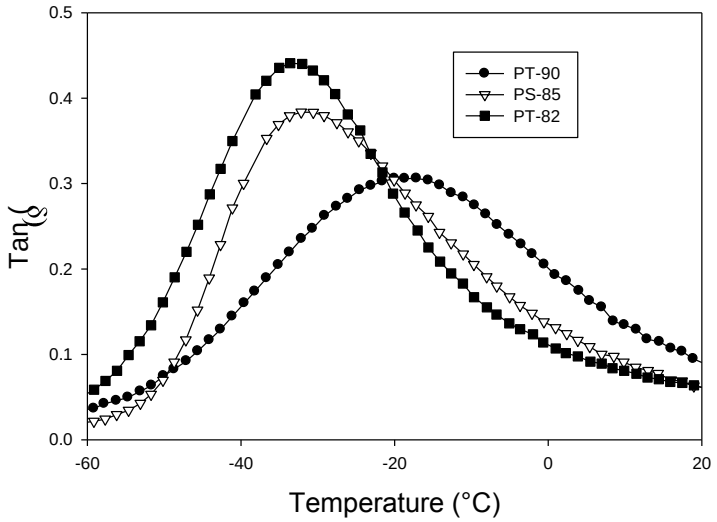

Figure 3.2 Variation of the Tan (δ) peak with hardness observed through DMA

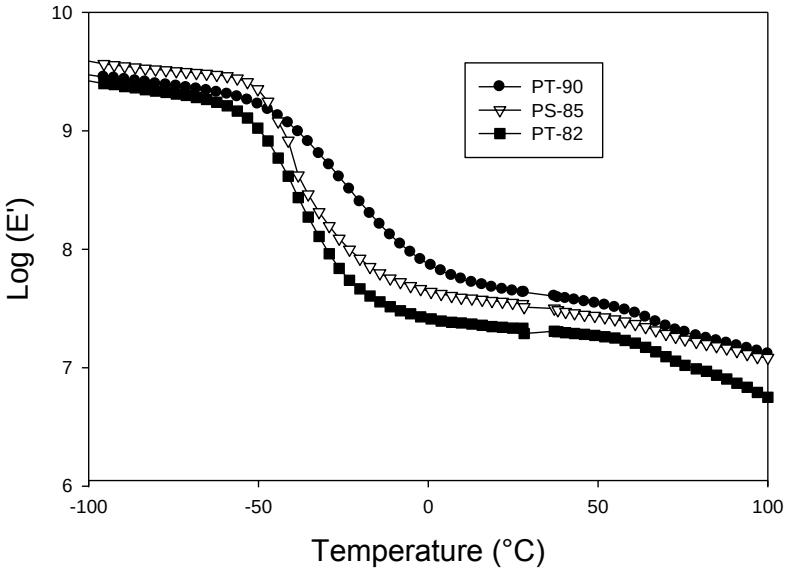

Figure 3.3 Variation of the storage modulus with temperature observed through DMA

3.1.3 Fourier Transform Infrared Spectroscopy (FTIR)

Figures 3.4 and 3.5 shows the FTIR results of the four polyurethane film samples. These results near N-H bond and C=O bond are considered to look for possible difference between the types of PU as well as their hardness. All the films showed peak only at 3340 cm^{-1} (bonded N-H) confirming that the urethane link is involved in the cross linking. There was clear difference in the FTIR results near the C=O bond between the polyester based and polyether based PU. The two polyester based films PS-80 & PS-85 showed a higher peak for both free C=O at 1730 cm^{-1}. Also, the free C=O peak is higher than the bonded C=O peak for polyester based PU films. In polyester based PU, the free C=O bond is found in the ester linkages of the soft segment whereas the bonded C=O (1730 cm^{-1}) is found in the urethane linkages of hard segment. However, in polyether there is no carbonyl linkages (C=O) in the ether linkages –(C-O-C)- and hence, both N-H and C=O represent the hard segment. The soft segment in the Polyether based PU is characterized by the –C-O-C- bond which gives peak at 1230 cm^{-1}. These FTIR results of the pristine film samples will be compared with the FTIR results of the eroded film samples and the extent of the damage in the bonds will be analyzed.

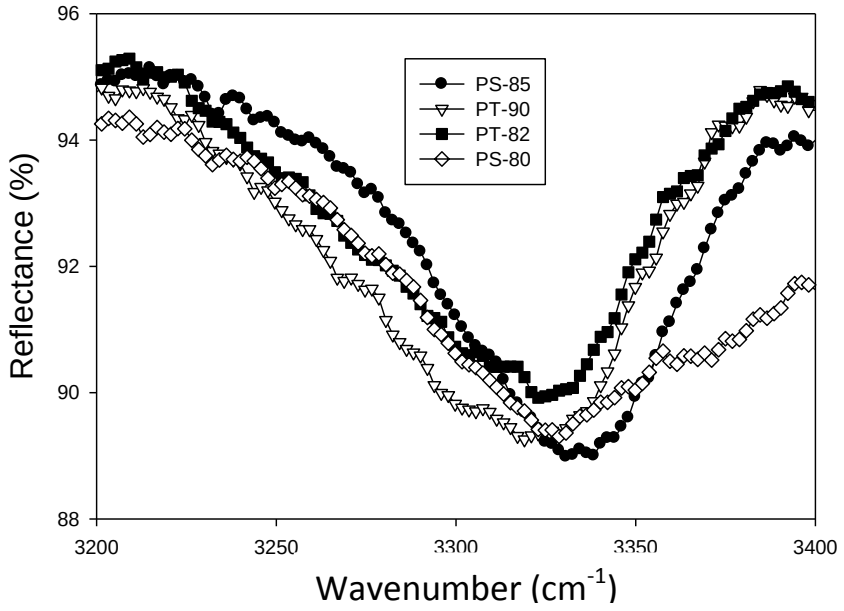

Figure 3.4 FTIR results of the polyurethane thin films near N-H region

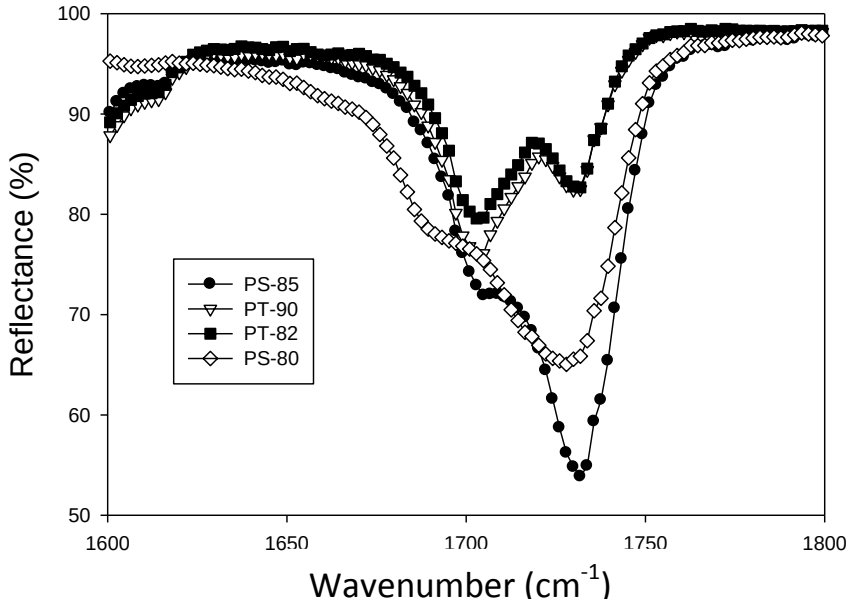

Figure 3.5. FTIR results of the polyurethane thin films near C=O region

3.2 Post Erosion Characterization

The PU films which were subjected to different stages of erosion have been studied through the DSC, FTIR and SEM to examine the damage in the micro structure.

3.2.1 Differential Scanning Calorimetry (DSC)

The DSC results of the pristine films corresponding to PT-90 when heated to 375°C revealed damage in the micro structure. The soft segment did not show melting peak in the first cycle because soft segment movement is hindered by the cross links between the hard and soft segments. The crosslink between the hard segments and soft segments is decomposed around 350°C. The soft segments which are melted during decomposition of the crosslink crystallize around 50°C on the cooling cycle up to -90°C. And because of that, the soft segments show a melting peak around 70°C in the second heating cycle. Figure 3.6 shows the complete two cycles of the DSC run for the PT-90 film.

More importantly, the DSC results of the PT-90 & PT-82 which are subjected to 0.5 g/cm^2 & 20 g/cm^2 erosion revealed the damage in the microstructure. The trend of gradual reduction in the melting peak corresponding to soft segments is seen when it is compared with the melting peak of pristine films. Figure 3.7 shows the comparison of the soft segments melting peaks during the second cycle for various mass loadings for PT-90 & PT-82 respectively. The reduction in the intensity of the peak clearly indicates the reduction in the crystalline portion of the soft segment after erosion.

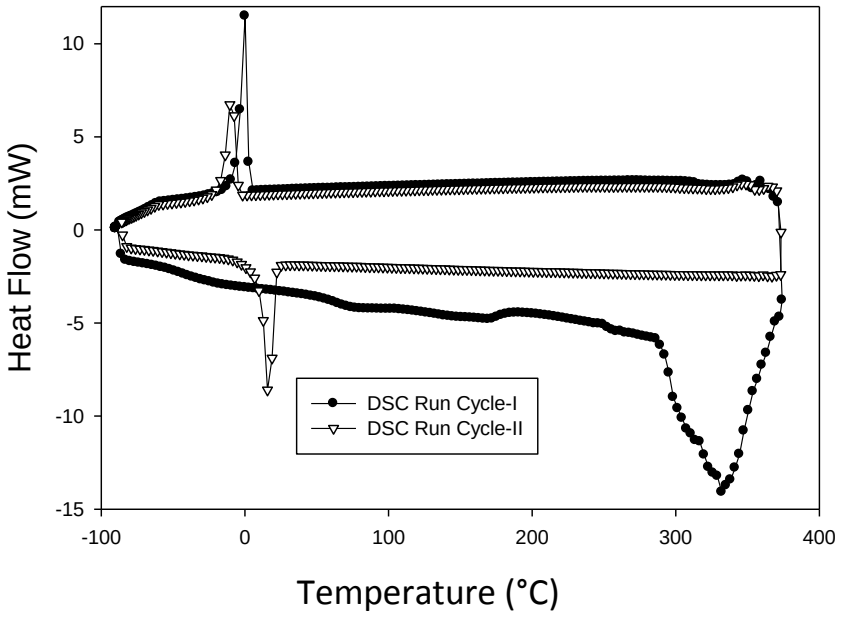

Figure 3.6 Two DSC cycles showing the melting peak in the 2nd cycle

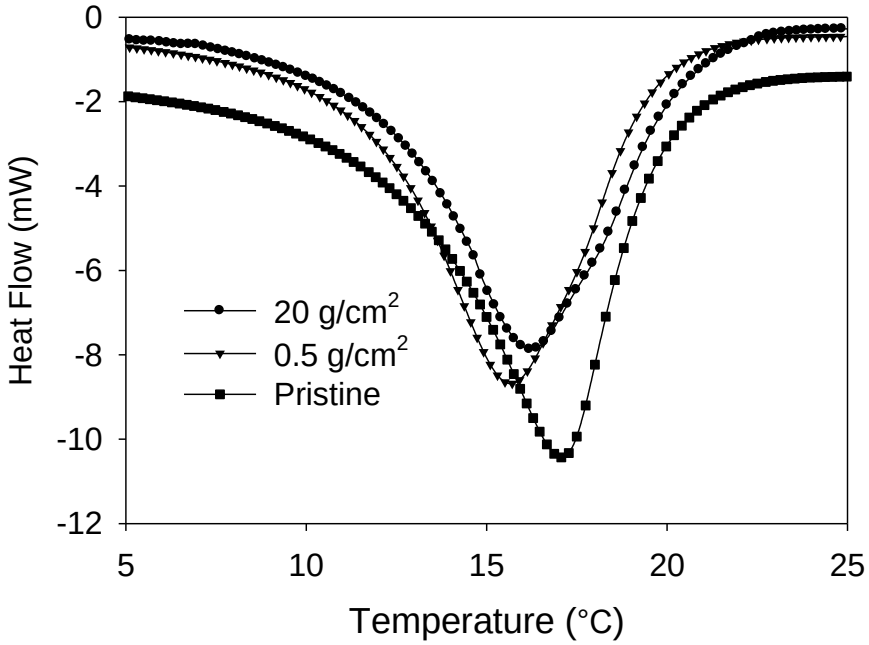

Figure 3.7 Soft segment melting peak for various mass loadings for PT-90

3.2.2 Fourier Transform Infrared Spectroscopy (FTIR)

The FTIR results of the eroded films of PS-80 and PS-85 subjected to various mass loadings indicate that the free C=O bond at 1730 cm^{-1} shows gradual reduction with the increase in the mass loading while the N-H bond at 3340 cm^{-1} which is found in the hard segments do not show any reduction as seen in the Figures 3.8 & 3.10 suggesting that the removal of the hard segment is very minimal. The reduction in the C=O bond is attributed to the change in the intensity of the peak as shown in Figure 3.9 & 3.11. However, the trend is different between the polyester and polyether based PU films. The polyester based PU films such as PS-80 & PS-85 which have significantly higher amount of free C=O have shown much reduction in the free C=O bond than the polyether based PT-82 & PT-90. These results suggest that the soft segment which contains the higher free C=O bonds in the polyester based PU has been removed from the surface gradually when the films are subjected to erosion and the damage is caused mainly during the early stages of erosion up to 2.0 g/cm^2.

PS-80 films which had more resistance to erosion than other films show in Figure 3.12 that there is a remarkable destruction of the free C=O bond corresponding to soft segments in them. Similarly, very minimum reduction of both the free and bonded C=O corresponding to hard segments is observed in the hardest film PT-90 in Figure 3.13, which suggests a correlation between the better erosion resistance and the part of the micro structure getting damaged. As we discussed earlier, there exists incubation period in the erosion in which material require more energy to roughen the surface after which steady state erosion takes place. The FTIR results showing the damage in the soft

segment at the earlier stages of erosion suggest that the high impact energy imparted on the surface of the films are getting absorbed by these macromolecular chains corresponding to soft segment. Additionally, because of the flexible nature of soft segment, these segments undergo ductile deformation and absorb more energy before they fail.

Damage in the micro structure in polyether based PU films is quite different. N-H bond and the C=O bonds (both free and bonded) did not show any reduction in the intensity of the peak. But, CH_2 (2860 cm^{-1}) and C-O-C (1250 cm^{-1}) groups show reduction due to erosion. The C-O-C bond represents the soft segment in polyether based PU films. The increase in the C-O (1100 cm^{-1}) groups seen in Figure 3.14 suggests that the group C-O-C has been broken down leading to the formation of more C-O. Apart from this, the C-N bond has also shown tremendous reduction due to erosion. Hence, it is likely that the breakage of the bonds had occurred gradually because of more exposure to sand particle impact. Apart from the damage in the soft segment part of the micro structure, some part of the hard segment or the crosslink which connect the two phases are getting damaged leading to the heavy amount of material removal when exposed to more than 20 g/cm^2. Mainly there are two possibilities for the location of the damage. First possibility is the breakage of the covalent bond C-N shown in the Figure 3.15 connecting the hard segment and the soft segment. Second possibility is the breakage of C-O-C bonds in the soft segment region leading to the small fragments of the soft segments on the surface of the eroded films. Zhang et al.[13] found using FTIR that the C-N

macromolecular chain was broken due to abrasion on the polyurethane. The C-N bond has the lowest bonding energy and is therefore most susceptible to failure due to impact.

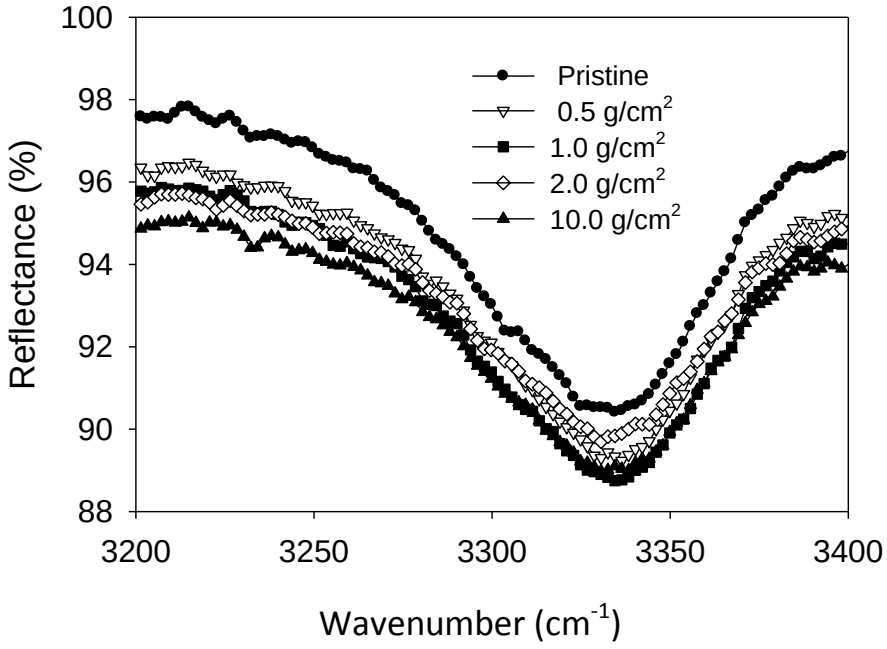

Figure 3.8 FTIR results near N-H region for different mass loadings of PS-85

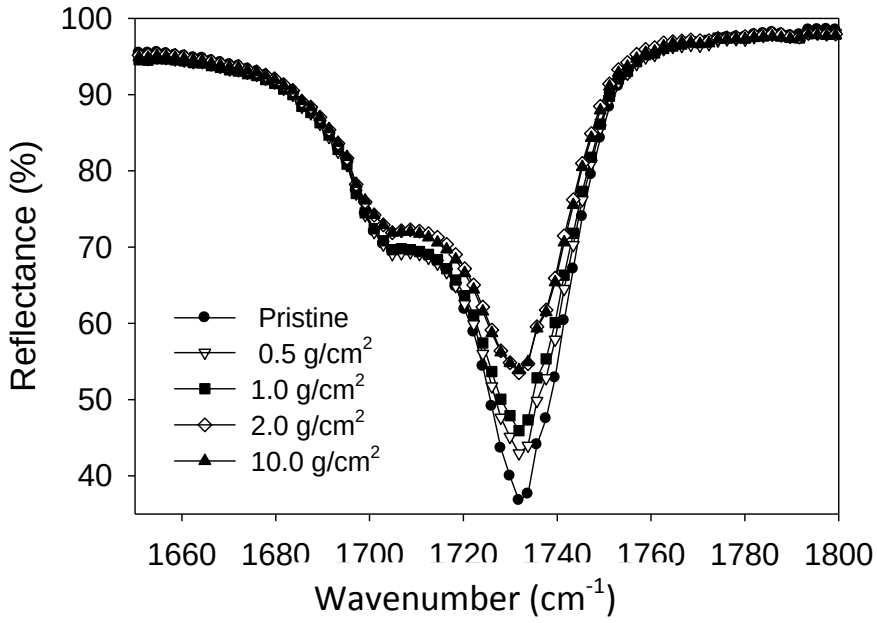

Figure 3.9 FTIR results near C=O region for different mass loadings of PS-85

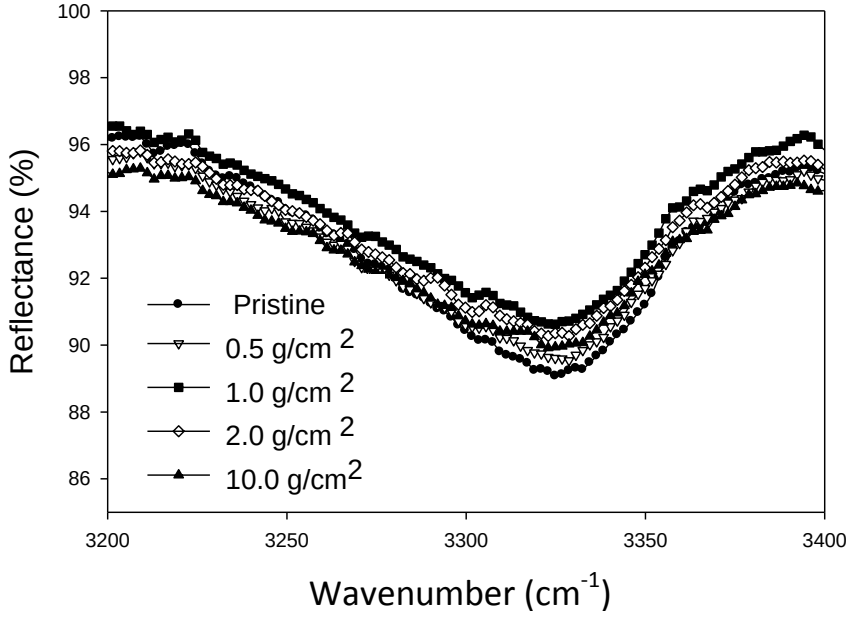

Figure 3.10 FTIR results near N-H region for different mass loadings of PT-82

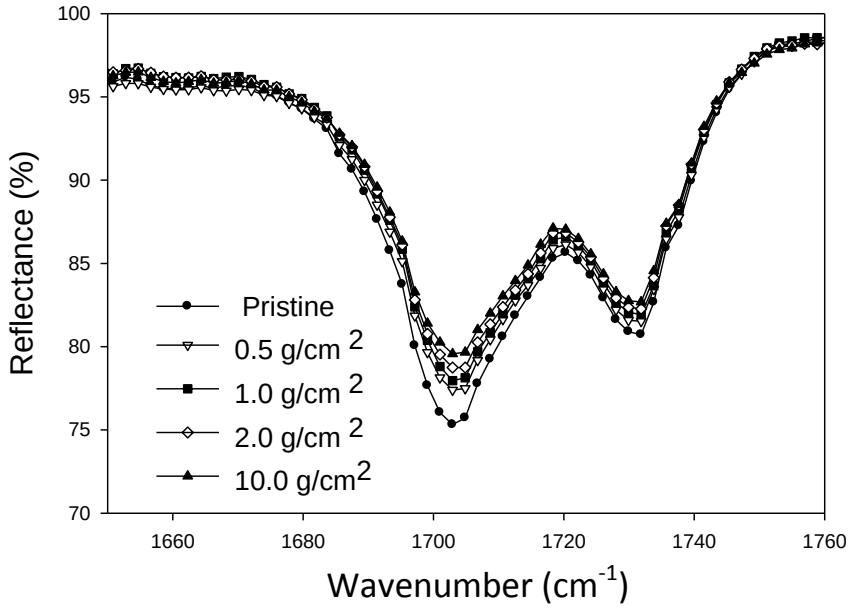

Figure 3.11 FTIR results near C=O region for different mass loadings of PT-82

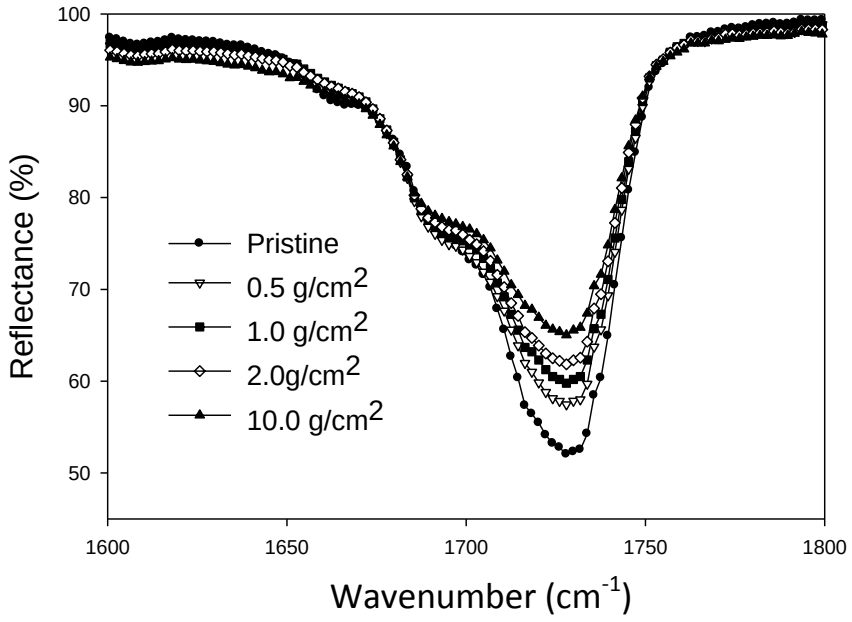

Figure 3.12 FTIR results near C=O region for different mass loadings of PS-80

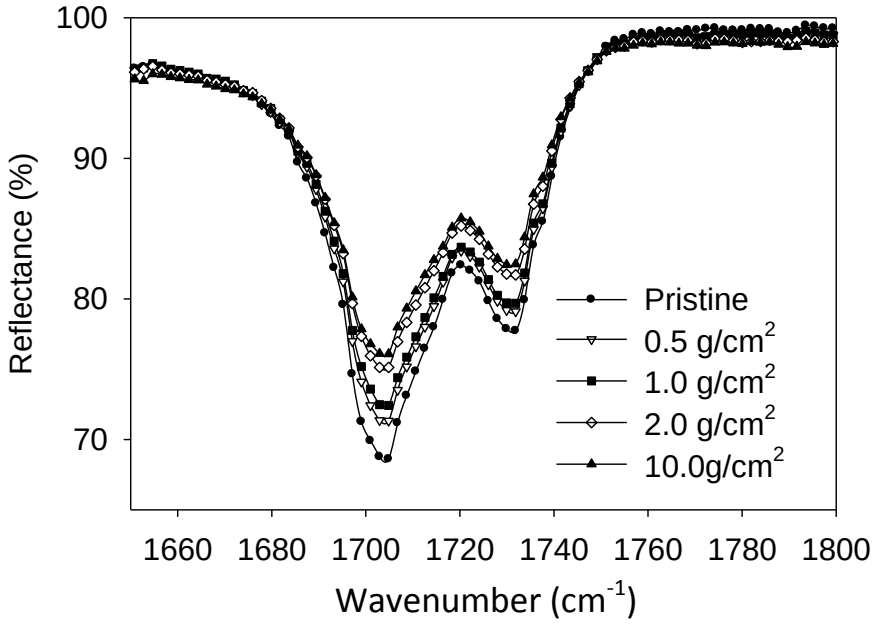

Figure 3.13 FTIR results near C=O region for different mass loadings of PT-90

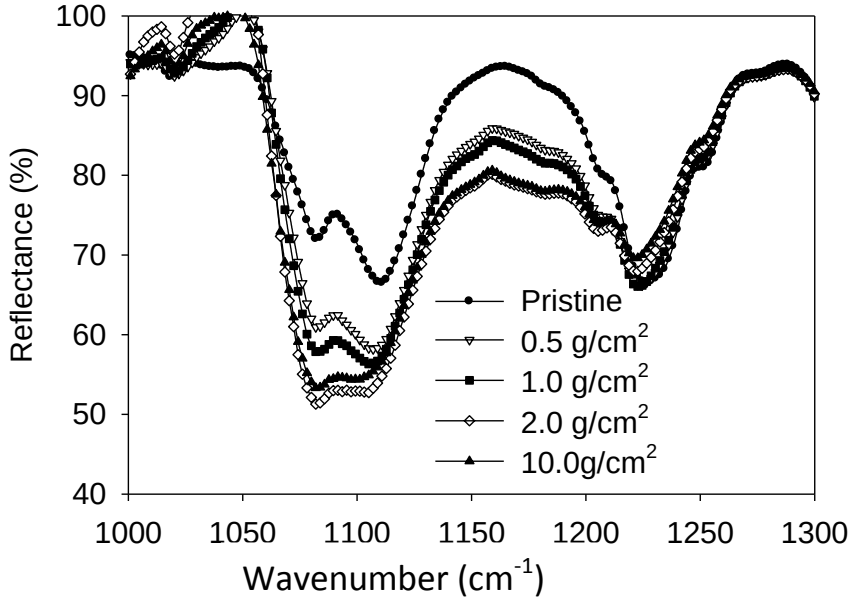

Figure 3.14 FTIR results near C-O-C & C-O region for various loadings of PT-90

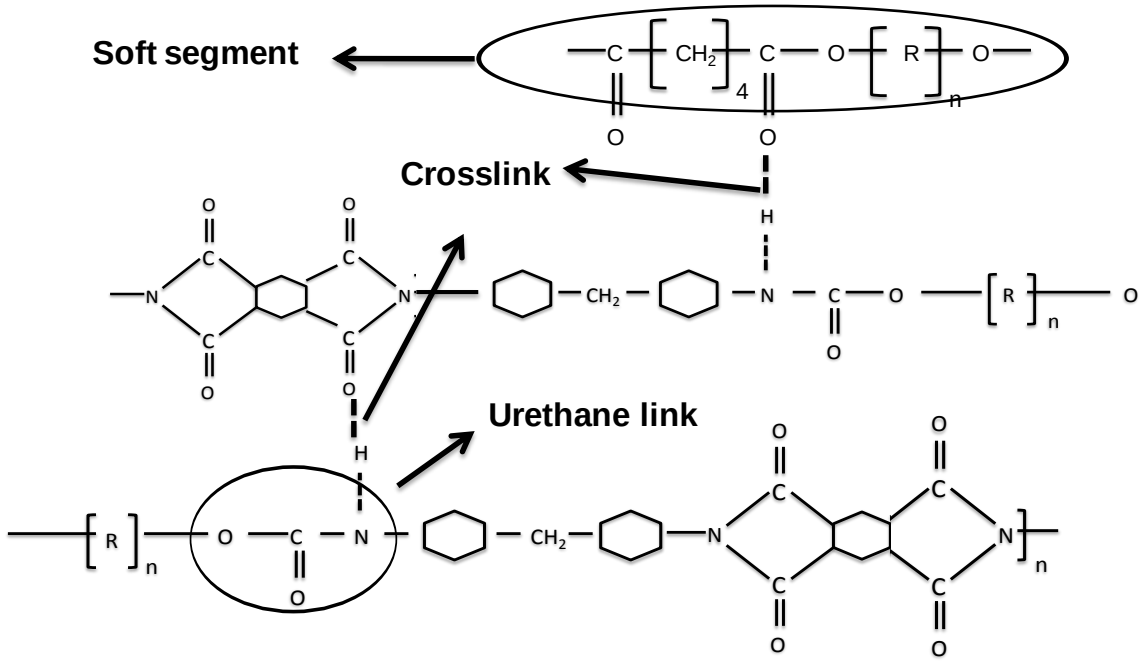

Figure 3.15. Chemical structure of PU showing cross links and urethane link

3.2.3 Scanning Electron Microscopy (SEM)

SEM was used to observe damage due to erosion on the surface of the eroded films by both Gulf (angular) and round sand. The energy dispersive spectroscopy (EDS) validated the existence of the minute silica particles embedded on the surface of the films.

SEM images were used to observe the sequence of damage in both polyester and polyether based PU as well as the variation of the surface damage between the softer and the harder films. Figure 3.16 shows the sequence of damage due to erosion by Gulf sand in the PS-80 films which has the best resistance to erosion. Initial stages showed more ductile deformation on the surface. The formation of the fragments is seen at the later stages and there is very less brittle cracking seen on the surface. Figure 3.17 shows the sequence of damage due to erosion by Gulf sand in the PS-85 films which has higher percentage of hard segments. The brittle cracks are seen at the second stage around 1.0 g/cm^2. Apart from the formation of fragments, the propagation of the brittle cracks is also seen around 20 g/cm^2.

The sequence of damage due to erosion by Gulf sand in the polyether based PT-82 is shown in Figure 3.18. Very little ductile deformation is observed during initial stages in which the bond breakage was noticed by FTIR on the PT-82. But, the density of the brittle cracks is higher than the PS-85 even though PT-82 has a lower hardness owing to the non-availability of the more free C=O bonds which are very flexible in nature. And the formation of fragments and the intersection of the brittle cracks are clearly visible at

the later stages. The film has undergone much damage due to erosion at 20 g/cm^2 with the evidence of rougher surface with huge cracks on the surface.

Similarly, the observation of the trend in the progress of damage due to erosion by Gulf sand in the PT-90 film is seen in Figure 3.19. The trend observed is similar to PT-82 being both polyether based PU. But, because of the higher hardness and higher hard segments, PT-90 had the most damage among all. Large numbers of brittle cracks which are relatively large are seen in the second stage. The final stage shows the material which is about to be removed due to the intersection of the cracks.

In general, polyester films show considerable amount of ductile deformation during the initial stages of erosion which correlates with the ductile deformation in the soft segment identified by FTIR. Formation of fragments, which mainly contain soft segments, is the primary mechanism of material removal in these films. On the other hand, polyether films did not show much of ductile deformation on the surface, instead brittle cracks are found during the initial stages of erosion. The intersection of the brittle cracks is the main mechanism of removal for these films. The formation of the brittle cracks was distinct for polyester and polyether based materials. And the material with high hardness shows high density of brittle cracks. Thus, the variation in the composition and the micro structure has changed the mechanism of erosion as observed in these films. And, the polyester based material with low hardness has shown good resistance to erosion, whereas the polyether based harder material has undergone huge damage.

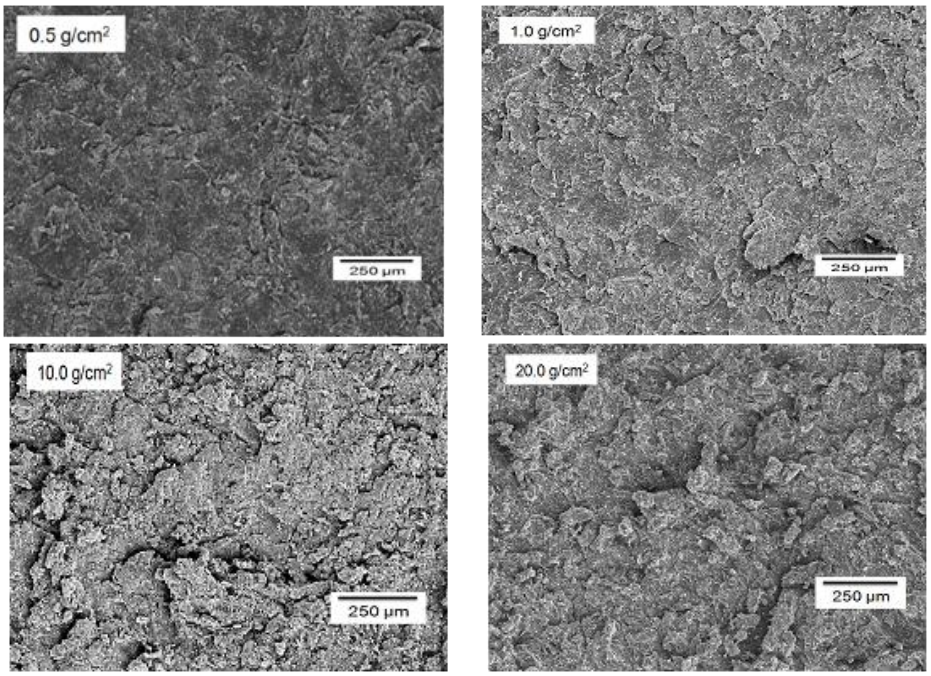

Figure 3.16 SEM images showing the stages of the erosion on PS-80 film surface

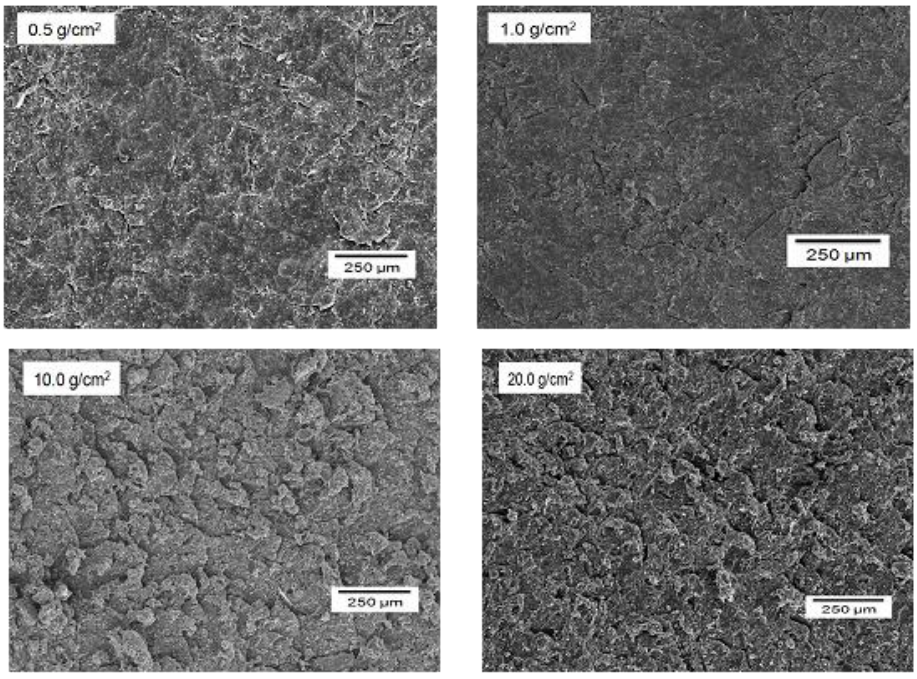

Figure 3.17 SEM images showing the stages of the erosion on PS-85 film surface

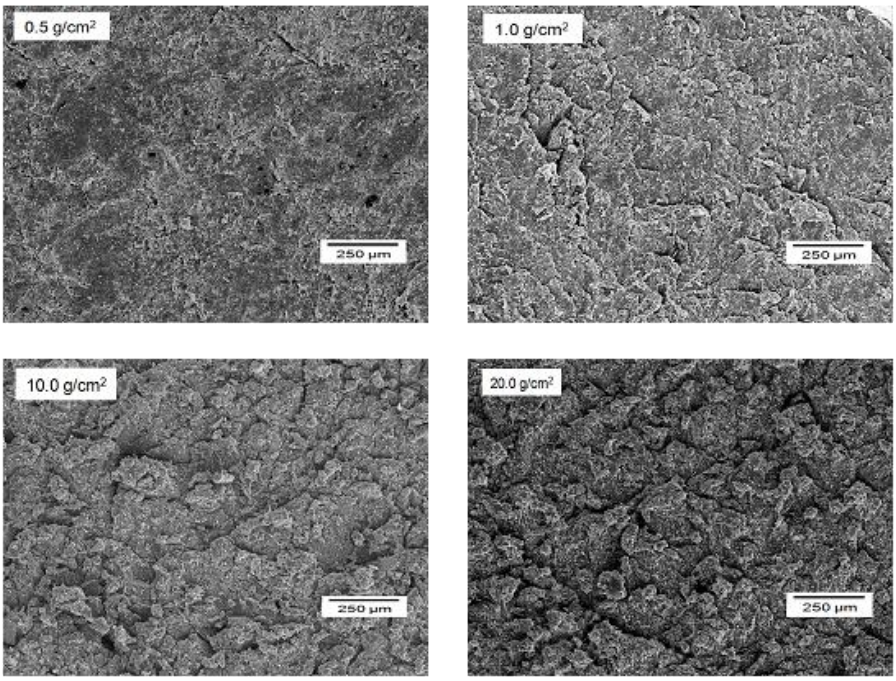

Figure 3.18 SEM images showing the stages of the erosion on PT-82 film surface

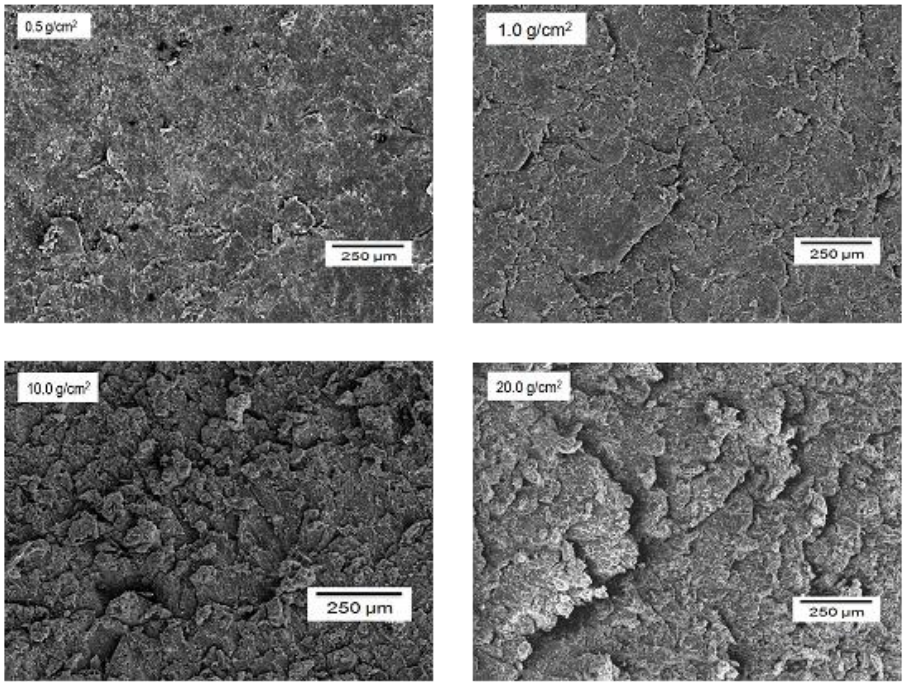

Figure 3.19 SEM images showing the stages of the erosion on PT-90 film surface

The SEM images at higher magnification revealed the change in the mechanism of erosion in PS and PT films. Figure 3.20 shows the fragments attached to the surface in PS film and the formation of brittle cracks in the PT film at initial stages of erosion at 1.0 g/cm^2 exposure of gulf sand. Similarly, at higher exposures Figure 3.21 shows the deformation of the material at the surface for the PS film, whereas the intersection of brittle cracks are visible for PT films.

The study was extended to observe the extent of damage in the bulk. The eroded films were broken under liquid nitrogen (LN_2) and the cross-section was viewed through SEM. The observations reveal that the damage on the surface had traveled into the bulk. The cracks formed due to the erosion traveling into the bulk as well as some brittle cracks were found in the cross-section. These cracks might have formed while the films were broken under LN_2. The cracks formed due to sand particle erosion were distinct from the brittle cracks formed. The brittle cracks formed due to breaking were so sharp that little or no gap was seen between the crack surfaces and also were not originating from the surface.

The propagation of the brittle crack formed on the surface into the bulk is seen in Figure 3.22. The crack has travelled into the bulk in a brittle manner with no plastic deformation near the crack tip. Apart from the big cracks in the bulk, the intersection of minute cracks beneath the surface is also visible in Figure 3.22. These two observations represent the two main ways of material removal, the intersection of brittle cracks in the bulk and the formation of fragments by the minute cracks beneath the surface.

Using the SEM images, the variation of the damage on the surface of the eroded films by the Gulf sand for different materials and different mass loading was observed. The effect of the damage by the round sand is also observed. Figure 3.23 (a-d) shows the surface of all the four films exposed to maximum loading by the gulf sand. The images reveal as expected that the damage is very minimal relative to the exposures to Gulf sand. The round sand media after 20 g/cm^2 exposure has just roughened the surface and no damage which can cause material removal is seen. And, there were no brittle cracks on the surface even for the hardest material. This implies that the brittle cracks on the films exposed to gulf sand might have been originated by the angular sand particles impinging on the hard segments on the surface.

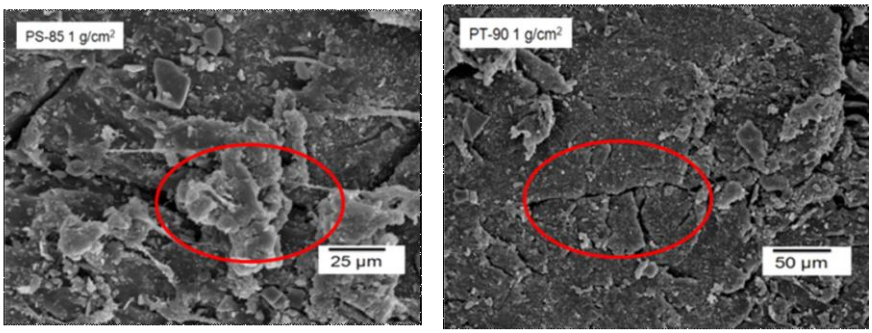

Figure 3.20 Comparison of initial damage in PS and PT films at earlier stages

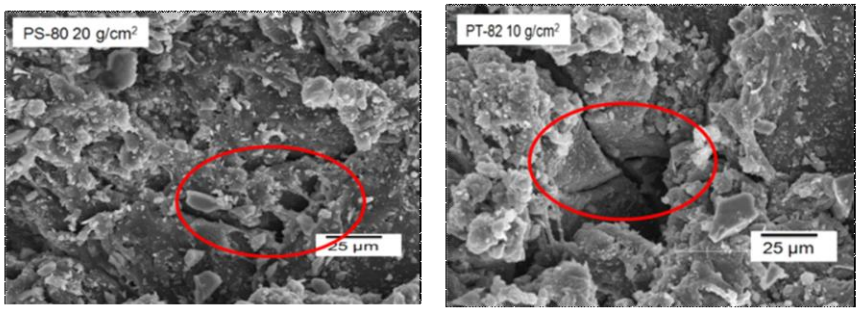

Figure 3.21 Comparison of damage at higher exposures in PS and PT films

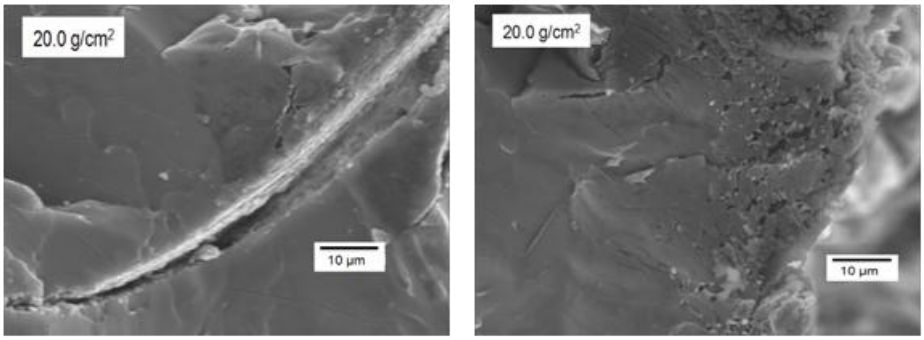

Figure 3.22 SEM images of cross section of the PT-90 film exposed to 20 g/cm^2

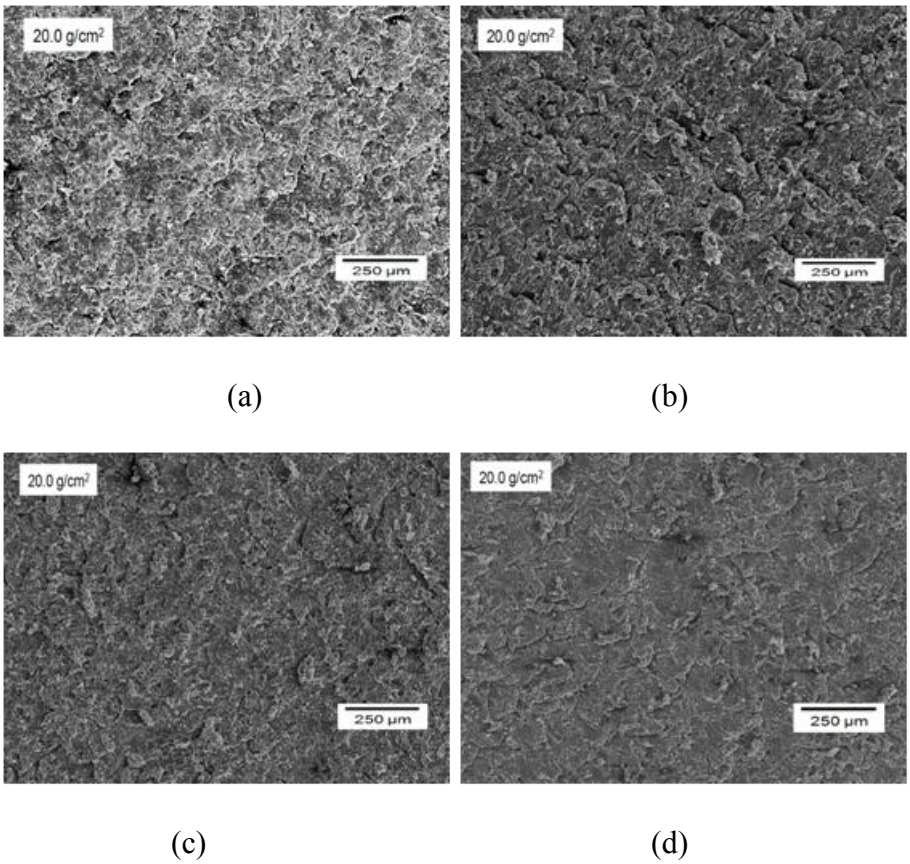

Figure 3.23 SEM images of films subjected to 20.0 g/cm^2 of round sand a) PS-80 b) PS-85 c) PT-82 and d) PT-90

4 SUMMARY AND CONCLUSIONS

The detailed investigations were done on both pristine and eroded PU films to detect the damage in the microstructure due to erosion. Initially, the thermal transitions of the pristine films were studied through Differential Scanning Calorimetry (DSC) and Dynamic Mechanical Analysis (DMA) yielding micro-scale information such as glass transition temperatures of the hard and soft segments. Furthermore, Fourier Transform Infrared Spectroscopy (FTIR) was utilized to document the signature of the pristine films. Sand particle erosion tests were carried out at 500 MPH, at an impact angle of 30° with two different sand media, round sand and golf sand. Test specimens were exposed to each sand media at different mass loadings ranging from 0.1 to 20 g/cm^2.

The tools of characterization used on the pristine polyurethane were once again used on the eroded specimens, with the goal to compare pre- and post- erosion findings. The FTIR results on the eroded films reveal the removal of macromolecular bonds corresponding to soft segments. In polyester based PU the trend in the reduction in the peak corresponding to free C=O and bonded C=O in the soft segments are seen whereas the N-H peak showed little or no reduction. In general, the polyester based PU showed good resistance to erosion as compared to polyether based PU. Using FTIR, free C=O bonds in the polyester based PU seem to decrease significantly, indicating that the bonds are breaking. This destruction of the C=O bonds suggests that damage in the soft segment leads to an overall better erosion resistance, as the soft segments are flexible and absorb

more impact energy before they fail. In polyether based PU the breakages of bonds such as C-O-C and C-N corresponding to soft and hard segments respectively are seen. The removal of these bonds from the surface of polyether based PU due to erosion is marginal as compared to the removal of free C=O bonds in the polyester based PU. The reduction of crystalline portion of soft segment observed from DSC results support the FTIR findings.

Scanning electron microscopy (SEM) images of the eroded specimens are used to correlate the sequence of the damage due to erosion to the PU micro structure. The observations revealed that after initial ductile deformation of the soft segments on the surface, brittle cracks are formed in the hard segments. The increased exposure to sand particles leads to formation of fragments containing mainly soft segments whereas the cracks in the hard segments tend to propagate in a brittle manner. When the intersection of the cracks happen at longer exposures, the material on the surface is removed, and it contains mainly soft segments as revealed by the FTIR and DSC results. Comparison of the sequences of the damage due to erosion between both the polyether and polyester based PU as well as the softer and harder material has been thoroughly carried out. The difference in the mechanism of erosion between the polyester and polyether based PU is shown in Figures 4.1 and 4.2. The low hardness polyester films show only ductile deformation at initial stages of erosion and the formation of fragments on the surface at higher exposures of sand. In the high hardness polyether based PU films, the damage initiates in the hard segments by formation of brittle cracks and further it is propagated into the bulk and intersected to form chunk of the material to be removed.

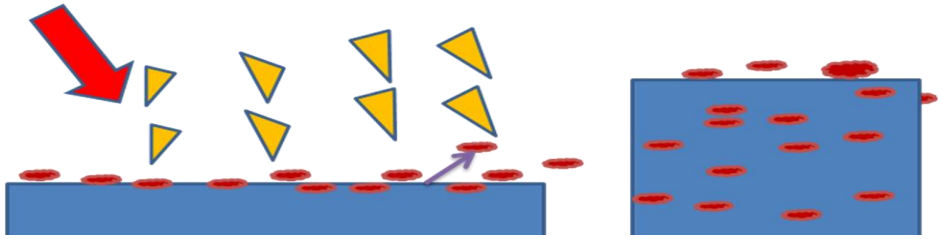

Figure 4.1 Mechanism of erosion in the polyester based low hardness PU films

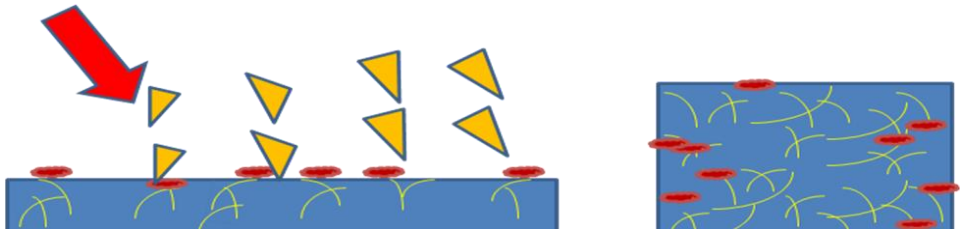

Figure 4.2 Mechanism of erosion in the polyether based high hardness PU films

From this comparison, possible reasons for better erosion resistance are discussed. The low hardness-polyester based material has shown good resistance to erosion whereas the polyether based harder material has undergone more significant damage. Presence of a larger number of free C=O bonds in the polyester based PU is thought to be the reason for this behavior since these free C=O bonds can absorb more energy through ductile deformation.

Thus, using the above techniques the observation of the breakage of the macromolecular bond as well as the ductile deformation and the cracks on the micro scale are seen. Mechanism of material removal has been mostly deduced using FTIR. The damage due to erosion starts with the bond breakage leading to various mechanisms such

as formation of fragments and intersection of brittle cracks which cause the material removal from the surface.

Future work will focus on the sequence of damage mechanism between the bond breakages and the role and source of micro cracks at the later stages of damage. In addition, it is suggested to investigate the following further: 1) the present study has focused on comparing different kinds of PU in terms of erosion resistance and its relation to the microstructure. A follow up study should focus on the same kind of PU, where the variation between samples is limited to microstructural variation such as in terms of %HS and SS to arrive at an understanding of effect of micro structure alone on erosion resistance. 2) Similarly, it is advised to focus on mechanism of erosion in the micro structure which happens immediately after the bond breakages before much developed mechanism like fragment formation and brittle cracks are seen on the surface. This will lead to a complete knowledge about the impact behavior of PU when it is subjected to sand particle erosion.

REFERENCES

Primary Sources

1. Hepburn, C. *Polyurethane Elastomers;* Applied Science Publishers: London, 1982.

2. Tocha, E.; Janik, H.; Debowski, M.; Vancso, G.J. *Journal of Macromolecular Science, Part B: Physics* **2002,** *41*, 4, 1291-1304.

3. Born, L.; Hespe, H.; Crone, J.; Wolf, K. H. *Colloid and Polymer Science* **1982,** *260,* 9, 819-828.

4. Hutchings,I.M.; J. Li. *Wear* **1990**, *135*, 293-303.

5. Preece,C.M.; Macmillan,N.H. *Annual Review Material Science* **1977,** *7*, 95-121.

6. Zahavi, J.; Schmitt, Jr, G. F. *Wear* **1981,** *71*, 2, 191-210.

7. Arnold, J. C.; Hutchings, I. M. In *International Conference on Wear of Materials,* **1989**, 99-107.

8. Hutchings, I. M.; Deuchar, D. W. T.; Muhr, A. H. *Journal of Materials Science* **1987,** *22*, 11, 4071-4076.

9. Spathis, G.; Niaounakis, M.; Kontou, E.; Apekis, L.; Pissis, P.; Christodoulides, C. *Journal of Applied Polymer Science* **1994,** *54*, 7, 831-842.

10. Lee, D.K.; Tsai, H.B. *Journal of Applied Polymer Science* **2000,** *75*, 1, 167-174.

11. ASTM Standard F1864-05, 2005, *Standard Test Method for Dust Erosion Resistance of Optical and Infrared Transparent Materials and Coating,* ASTM International, West Conshohocken, PA, **2005**, DOI: 10.1520/F1864-05, www.astm.org.

12. Woo, E. J.; Farber, G.; Farris, R. J.; Lillya, C. P.; Chien, J. C. W. *Polymer Engineering and Science* **1985,** *25*, 13, 834-840.

13. Zhang, S. W.; He, R.; Wang, D.; Fan, Q. *Journal of Materials Science* **2001,** *36*, 20, 5037-5043.

14. Hodzic, A.; Stachurski, Z. H.; Kim, J. K. *Polymer* **2000,** *41*, 18, 6895-6905.

Secondary Sources

15. Mishra, A. K. *Progress in Organic Coatings* **2006,** *55*, 3, 231-243.

16. Liu, J.; Ma, D.; Li, Z. *European Polymer Journal* **2002,** *38*, 4, 661-665.

17. Arjula, S.; Harsha, A.; Ghosh, M. *Journal of Materials Science* **2008,** *43*, 6, 1757-1768.

18. Vu-Khanh ,T.; De Charentenay, F. X. *Polymer Engineering & Science* **1985,** *25*, 13, 841-850.

19. Zebarjad, S. M.; Lazzeri, A.; Bagheri, R.; Seyed Reihani, S. M.; Frounchi, M. *Materials Letters* **2003,** *57*, 18, 2733-2741.

20. Xia, H.; Song, M.; Zhang, Z.; Richardson,M. *Journal of Applied Polymer Science* **2007,** *103*, 5, 2992-3002.

21. Leung, L. M.; Koberstein, J. T. *Journal of Polymer Science. Part A-2, Polymer Physics* **1985,** *23*, 9, 1883-1913.

22. ASTM Standard D882-09, 2009, *Standard Test Method for Tensile Properties of Thin Plastic Sheeting,* ASTM International, West Conshohocken, PA, **2009** DOI: 10.1520/D0882-09, www.astm.org.

APPENDIX A

Nano-indentation

Properties such as hardness and elastic modulus can be obtained by nano-indentation and this method is very sensitive to the composition of the polyurethane elastomer. Based on the diisocyanates and polyethers/polyesters used and the amount of the crystalline portion in the hard segment the nano-scale properties change. Usually, these properties show bi-modal distribution corresponding to the soft and hard segments.

Hodzic et al.[14] have performed nano-indentation on the glass fiber polyester composite in order to distinguish the properties of the inter-phase region. As shown in Figure A.1, depending upon the phase on which the indentation occurs, it showed very different loading and unloading curves.It was possible to clearly identify the portion of the composite which belongs to the interphase region which has the mechanical properties in between the polyester and the glass fiber. Polyurethane which exhibits multi-phase separation is expected to give more distributed nano-scale properties during the nano-indentation.

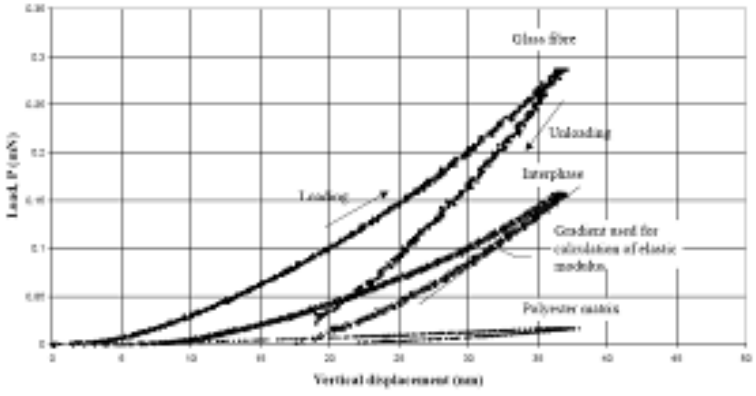

Figure A.1 Nano-indentation loading/unloading curve of a polymer composite[14]

Tocha et al.[7] showed that the crystalline portion of hard segment leads to multi-phase dispersion with two or more phases of the crystalline structure of the hard segment present. Due to this, it is expected that the nano-scale properties of polyurethane would change considerably depending on where the indentation takes place, either in the spherulites or in the portion away from the spherulites, showing the nano-scale dispersion. In order to get the distribution for the PU films under consideration, we have carried out a series of nano-indentation experiments by varying the separation distance between each point of indentation and the modal distribution corresponding to PT-82 film is shown in Figure A.2. This indicates the multi-phase properties in polyurethane films.

Similar nano-indentation experiments were carried out for the three polyurethane samples, and the distribution of the nano-scale properties were obtained. Figure A.3 shows the variation in the load-displacement curves at different indentation points. Some of the indentation tests were done by holding the maximum load for 10 seconds and 30 seconds, respectively, to see the effect of the stress relaxation in the unloading curve.

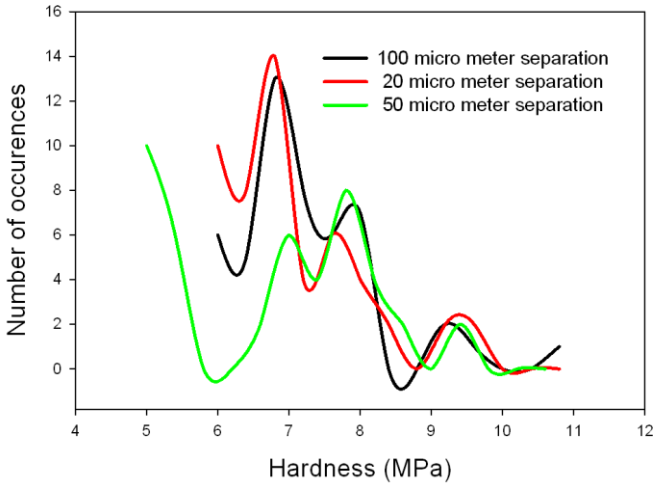

Figure A.2 Modal distribution of the hardness of PT-82

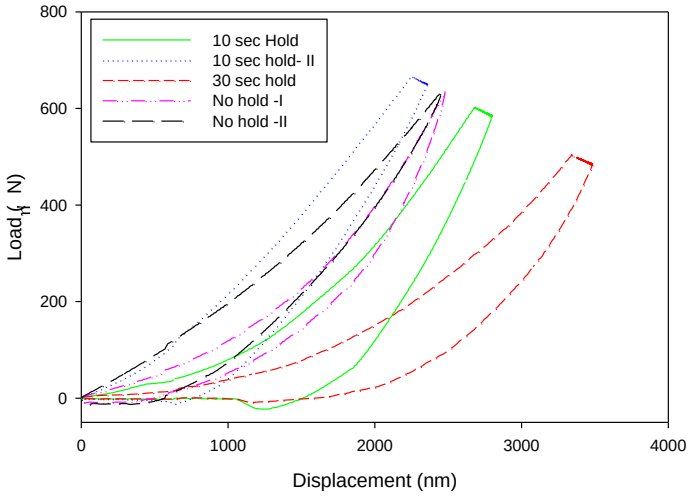

Figure A.3 Load –displacement curves for PS-85

APPENDIX B

Lee et al. [10] studied the variation of the mechanical properties for different diisocyanates. As expected, the choice of the diisocyanate and the proportion of it played a vital role in the stress-strain curves of the polyurethane. The table gives the tensile strength, Young's modulus, the elongation at break and the shore hardness for various PU. The stress-strain curves are shown in Figure B.1. There is a good correlation between the hardness and the young's modulus, showing that high Shore A hardness gives high modulus. This is because, the percentage of the hard segment controls both these properties of PU. However, there is no direct relation between the tensile strength and the hardness because, apart from the percentage of the hard segment, the crystallinity and the crystal parameters of the hard segment influence the tensile strength of PU.

Table 5 Properties of the various polyurethanes with different diisocyanates

Sample	Young's Modulus (MPa)	Tensile Strength (MPa)	Elongation at Break (%)	Shore A Hardness	Tear Strength (kN/m)
MDI-40	49.3	42.9	1160	96	139
T100-40	18.7	16.8	1480	80	64
T80-40	17.5	14.0	1290	77	61
IPDI-40	17.8	9.5	1280	75	55
HMDI-40	43.6	24.3	710	94	110
HDI-40	40.5	10.4	200	94	76

All segmented polyurethanes except HDI-40 show ductile behavior and have elongation at break of more than 700%. The HDI-40 shows brittle behavior and poor mechanical strength because of its very high crystallinity. The polyurethanes with

symmetrical hard segment such as HDI-40, MDI-40 and HMDI-40 have higher Young's modulus and hardness.

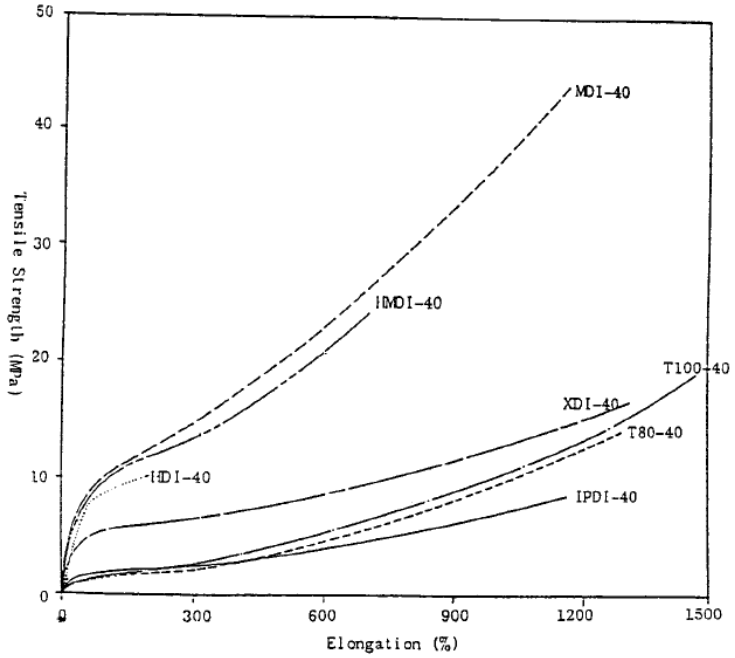

Figure B.1 Stress-strain curves of the different polyurethane[10]

The Tensile tests were carried out on the thermoplastic pure polyurethane samples PS-85, PT-82 & PT-90. The ASTM standard D-882-09 was followed to test the thin film samples of polyurethane. The tests were carried at room temperature. The loading and unloading curves were plotted up to 300 % strain. Three different strain rates of 0.001, 0.01 and 0.1 mm/mm-min were used and the all the stress-strain curves were compared for the behavior of the polyurethane at different testing conditions. The tests are done at three temperatures: 25°C, 50°C and 85°C and the stress-strain curves for the PS-85 film are shown in Figures B.2-B.4.

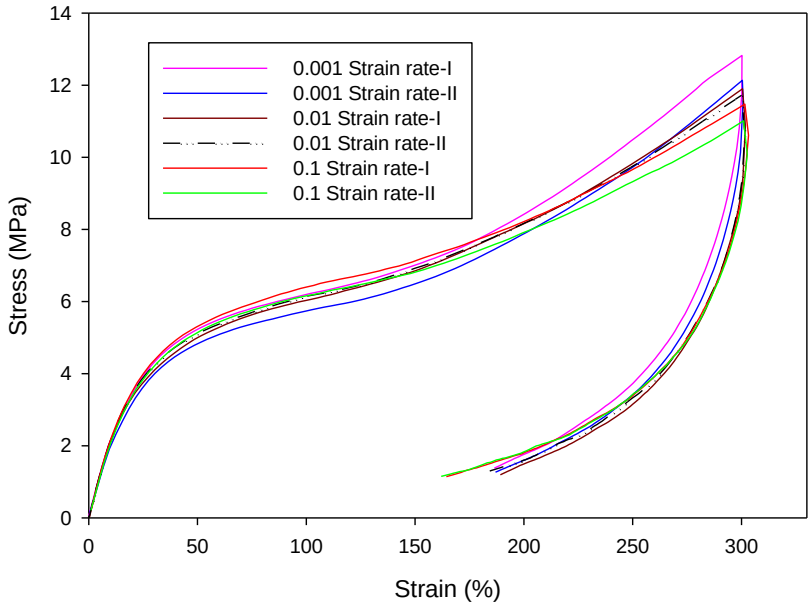

Figure B.2 Stress-strain curves of PS-85 at different strain rates at 25°C

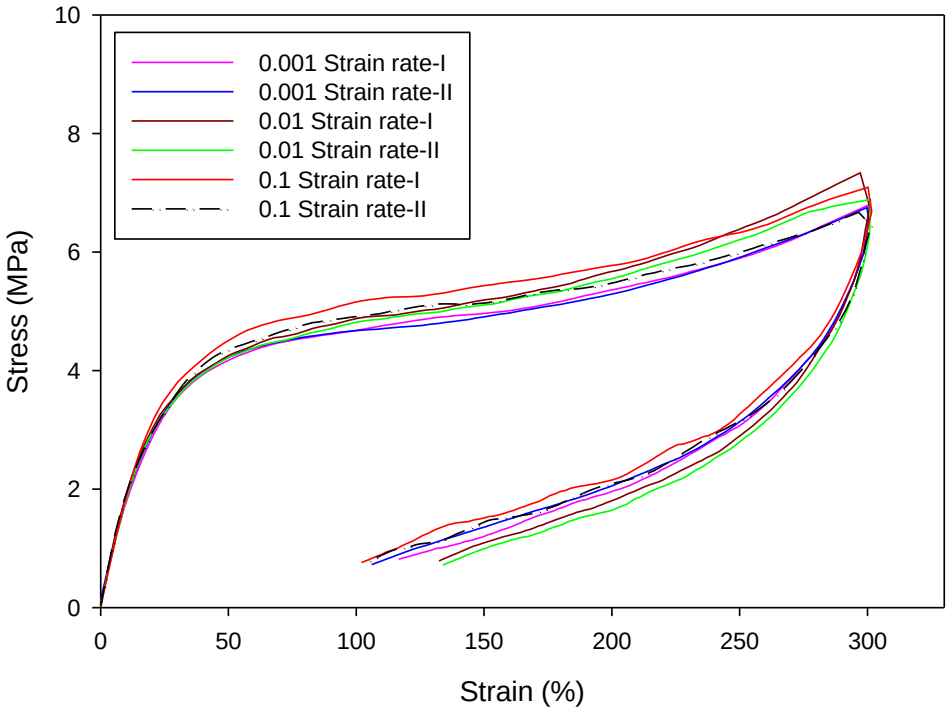

Figure B.3 Stress-strain curves of PS-85 at different strain rates at 50°C

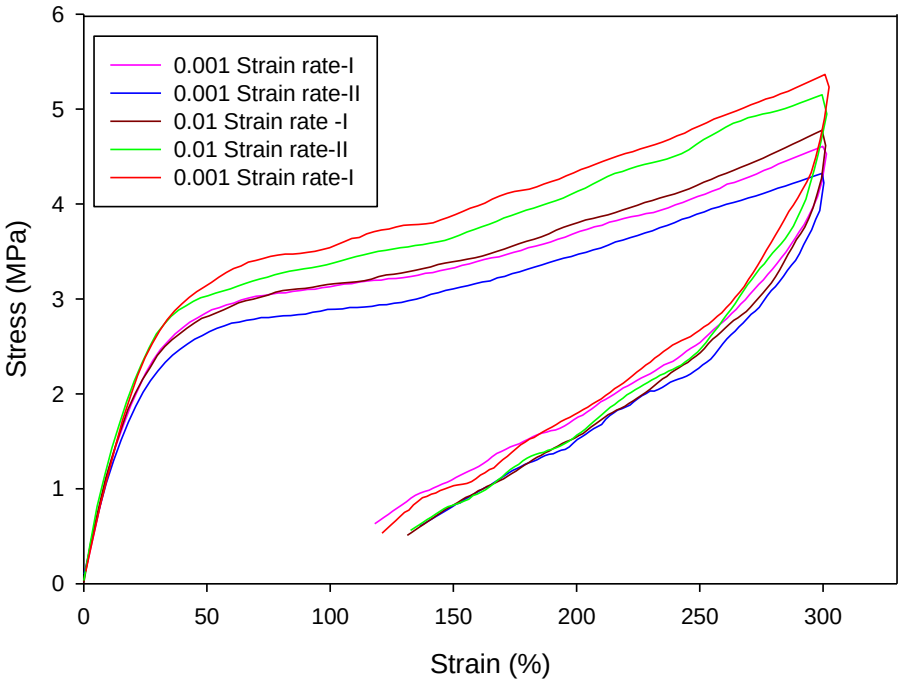

Figure B.4. Stress-strain curves of PS-85 at different strain rates at 85°C

VITA

Nirmal Shankar Sigamani obtained a B.Tech. degree in aerospace engineering from Anna University, India in the spring of 2004. He worked at the Gas Turbine Research Establishment, Bangalore,for four years. He joined the M.S. degree program in aerospace engineering under the guidance of Dr. Zoubeida Ounaies and Dr. Ramesh Talreja during the Fall of 2008 and graduated in May 2010. His primary interest is in the area of impact damage characterization of polymers and the evaluation of damage in micro structure due to solid particle erosion.

Nirmal can be reached at: Aerospace Engineering, Texas A&M University, College Station, TX, 77843-1226. His email address is nirshank@gmail.com.